land

MDPI

Article

A Dual-Layer Complex Network-Based Quantitative Flood Vulnerability Assessment Method of Transportation Systems

Jiayu Ding [1,2], Yuewei Wang [2,3,*] and Chaoyue Li [1]

[1] School of Future Technology, China University of Geosciences, Wuhan 430074, China; ding_jiayu@cug.edu.cn (J.D.); lcyhxy@cug.edu.cn (C.L.)
[2] Hubei Key Laboratory of Intelligent Geo-Information Processing, China University of Geosciences, Wuhan 430074, China
[3] School of Computer Science, China University of Geosciences, Wuhan 430074, China
* Correspondence: yuewei.w@cug.edu.cn

Abstract: Evaluating the vulnerability of urban transportation systems to flood disasters can provide scientific support for urban disaster prevention and mitigation. Current methods for assessing the flood vulnerability of urban roads often overlook the internal relationships within the complex spatial composition of road networks and surface structures. In this study, based on the theory of complex networks, a dual-layer network assessment model is established for evaluating the flood vulnerability of urban transportation systems by coupling basic geographic data with road network vector data. Unlike traditional methods, this model considers the complex relationship between road network structures and ground surfaces, uncovering a correlation between road network structure and road flood vulnerability. By utilizing this model, the flood vulnerability of road networks in Shenzhen, as well as the city's spatial flood vulnerability, are quantitatively assessed. Based on the quantitative results, we create maps illustrating the distribution of road and spatial flood vulnerability in Shenzhen. The study results reflect that roads highly vulnerable to flooding are mainly located in the central urban area of the southwest, with the flood vulnerability spatially concentrated primarily in the northern and western regions. Using data from government reports, news stories, and other sources over the past five years, we compile recorded instances of urban waterlogging. The quantitative results of the model are consistent with the distribution trend in recorded waterlogging points, indicating that the model's outcomes are authentic and reliable.

Keywords: flood vulnerability; complex network; remote sensing; urban waterlogging; dual-layer network; risk assessment

check for updates

Citation: Ding, J.; Wang, Y.; Li, C. A Dual-Layer Complex Network-Based Quantitative Flood Vulnerability Assessment Method of Transportation Systems. *Land* **2024**, *13*, 753. https://doi.org/10.3390/land13060753

Academic Editors: Leila Hashemi Beni and Aqil Tariq

Received: 11 April 2024
Revised: 23 May 2024
Accepted: 25 May 2024
Published: 28 May 2024

Copyright: © 2024 by the authors. Licensee MDPI, Basel, Switzerland. This article is an open access article distributed under the terms and conditions of the Creative Commons Attribution (CC BY) license (https://creativecommons.org/licenses/by/4.0/).

1. Introduction

Floods are significant natural disasters that occur frequently on a global scale, posing serious threats to human lives and societal progress [1,2]. In China, floods have triggered numerous major disaster events, resulting in casualties and economic losses, especially in urban areas [3,4]. With the acceleration of urbanization in China, the increasing population, dense built-up areas, and complex road networks are more susceptible to flood impacts [5]. Therefore, conducting urban flood disaster risk assessments becomes particularly important to better formulate emergency response plans for flood disasters and reduce the impact of such disasters [6].

Flood disaster risk assessment is one of the fundamental bases for developing disaster prevention plans and has been extensively studied in recent years. The main research methods are divided into the multi-criteria index system method, the coupling of remote sensing and GIS, and scenario simulation assessment [7]. The multi-criteria index system is the most widely used method for flood risk assessment [8]. Based on the natural characteristics and socioeconomic specifics of the study area, this approach selects relevant direct and indirect index factors for urban flood disasters, constructs a flood risk assessment index system,

and uses mathematical models to evaluate and define the overall flood risk [9]. The method based on the coupling of remote sensing and GIS uses remote sensing technology to obtain information such as water area, inundation duration, and disaster-bearing bodies in the disaster area, and then, inputs this information into GIS tools for spatial analysis [10]. Based on hydrological and hydrodynamic models, scenario simulation assessment is a method for dynamic simulation and assessment of disaster processes in the study area by designing disaster scenarios of specific frequency and intensity (design rainfall) [11]. In recent years, a large number of researchers have begun to experiment with machine learning methods for flood risk assessment. These rely on intelligent algorithms to learn the characteristics of flood risk and automatically acquire the input–output relationship between driving factors and flood risk [12]. These methods provide different ideas for flood hazard assessment.

Flood risk is commonly understood as a function of three components: hazard—the likelihood of a flood occurring; exposure—the number and value of assets at risk; and vulnerability—the ability of a society to respond to the event [13,14]. Although our comprehension of hazard and exposure has significantly advanced over time, understanding vulnerability continues to be a major challenge in flood risk assessment today [15,16]. Over the past few decades, flood vulnerability has been an important indicator for assessing the impact of flood disasters in a region, holding significant research value [17,18].

Vulnerability, the core indicator for measuring the extent of a disaster's impact, refers to the potential damage that a system can incur under the influence or pressure of a disaster [19]. Therefore, flood vulnerability analysis does not mean analyzing a single likelihood of exposure, but it requires a comprehensive analysis of the extent of exposure damage. It includes a wide range of social, economic, and other characteristics that affect the sensitivity of the exposed elements to the impact of the disaster [20,21]. Because of the importance of flood vulnerability analysis, international initiatives, such as the Sendai Framework for Disaster Risk Reduction 2015–2030 (United Nations International Strategy for Disaster Reduction, 2015), emphasize the need to understand and evaluate flood vulnerability [22]. Flood vulnerability assessment plays a crucial role in flood risk assessment [17].

Scholars have analyzed flood vulnerability from different perspectives and obtained important results [23]. In conducting spatial flood vulnerability assessments, index-based models or situational simulation models are commonly used for the analysis. In the context of index-based models, Brouwer et al. [24] investigate local-scale flood risk and resilience to assess the extent of flood exposure in Malaysia and how people respond to flood damage. Xuerao et al. [19] construct an evaluation model for urban flood disaster vulnerability by considering exposure, sensitivity, and adaptability, and assess urban flood vulnerability using the entropy method. In the realm of situational simulation models, Suarez et al. [25] evaluate the impact of flooding and climate change on Boston's urban transportation system through situational simulation assessments. Utilizing actual measurement data and maximum water depth survey results, Jiake et al. [26] establish an accurate coupled model of floods in the study area to simulate current and design scenarios, and evaluate flood disaster vulnerability according to the simulation results.

In addition, the study of the vulnerability of transportation systems should be given significant attention. The focus of this paper is on one specific critical infrastructure system—the transport system. The road system, in particular, is fundamental to the functioning of society in both developed and developing countries [27]. A transportation system can be defined as a highly dynamic network composed of various vehicles and infrastructure such as roads [28]. Due to the high susceptibility of transportation systems to extreme events, assessing their vulnerability is of utmost importance [29]. In assessing the vulnerability of transportation systems, most studies focus on the analysis of networks' structural characteristics. For example, Balijepalli et al. [30] examine the vulnerability of urban road networks in maintaining connectivity. In another study, Santos et al. [31] explore the vulnerability of roads in mitigating the impact of floods from the perspective of network efficiency. These studies provide options for flood vulnerability assessment based on different perspectives. Additionally, some studies analyze the flood vulnerability

of transportation systems using scenario simulation models. Abdulla et al. [32] model and characterize seepage dynamics in road networks during major river flood events to evaluate flood vulnerability. Prasoon et al. [33] simulate multiple rainfall events, map road network inundation, and assess the spatial vulnerability of the road network.

Although disaster vulnerability assessment methods have shown a certain degree of maturity, they commonly rely on the direct overlay of diverse geographic data, which significantly limits their accuracy [34–36]. Particularly in assessing road network vulnerability to flooding, past research often failed to fully account for the crucial element of complex spatial interconnectivity between network structures and surface composition. Additionally, due to the inherent diversity of multisource geographic data, traditional methods struggle to accurately integrate these varied datasets, posing challenges in effectively organizing different geographic information components [37].

To address the challenges mentioned above, this study combines various assessment algorithms to construct a dual-layer complex network model based on multisource geographic data. In this model, a method for assessing urban road flood vulnerability and spatial flood vulnerability is proposed. Unlike traditional research methods, our proposed approach utilizes a dual-layer network structure to analyze the complex relationship between road network structures and surface conditions thoroughly. It systematically organizes various types of data to conduct a scientific analysis of urban road flood vulnerability. This research considers multiple factors, including natural disaster-causing elements and human factors, to make the assessment results more scientific and standardized. To our knowledge, our research is the first to provide a solution for flood disaster vulnerability assessment based on a multi-layer complex network, offering an innovative approach. The primary contributions of this research are summarized as follows:

1. Propose a dual-layer network model for flood vulnerability assessment based on complex network theory.
2. Integrate the interconnection between road networks and surface conditions into the assessment.
3. Apply the assessment model to evaluate spatial and road flood vulnerabilities in Shenzhen.

The rest of this paper is organized as follows. Section 2 introduces the research data and methods. Section 3 presents the research findings on Shenzhen as the study area. Section 4 describes the experiments conducted to evaluate the efficacy of the proposed method, presents a comparative analysis with related research methods, and provides suggestions for reducing flood vulnerability. Section 5 concludes the paper.

2. Materials and Methods

Based on the research background, this section introduces the details of the proposed study. Section 2.1 describes the details and sources of the data. Section 2.2 presents the overall methodology of the study, and Sections 2.3 and 2.4 discuss the research methods in depth.

2.1. Dataset

The dataset for this study includes remote sensing data and basic road data. The remote sensing data include natural categories such as rainfall and elevation, as well as economic categories like night lighting and building heights. These factors influence disaster susceptibility and disaster-induced losses, all of which are related to flood vulnerability [38–42]. Additionally, the basic road data incorporate various types of geographic information data, which should also be reasonably included in the study [43]. For example, the traffic volume of roads affects the efficiency of the transportation system, which in turn impacts the system's vulnerability [44]. These data, which have a high correlation with the flood vulnerability of the system, are selected to be included in the study dataset.

The data come in different types, such as raster and vector data. The types and sources of the data used are presented in Table 1.

Table 1. Names and sources of study area base data.

Data Name	Data Type	Details	Data Source
Elevation	Raster data	2009, 30 m resolution	Geospatial Data Cloud
Rainfall	Raster data	2021, 30 m resolution	National Meteorological Science Data Center, China
CLCD [1]	Raster data	2021, 30 m resolution	National Earth System Science Data Center
Nightlight	Raster data	2021, 1000 m resolution	National Centers for Environmental Information (NCEI)
Population density	Raster data	2020, 1000 m resolution	WorldPop
Building height	Raster data	2023, 10 m resolution	CNBH Dataset [45]
Water distribution	Vector data	2021	OpenStreetMap
Road network	Vector data	2021	OpenStreetMap
Traffic flow	Attribute data	2023	Shenzhen Road Traffic Operation Index System
Lane information [2]	Attribute data	2023	Shenzhen Housing and Construction Bureau

[1] CLCD: China Land Cover Dataset [46]. [2] Lane information encompasses data on lane width, lane grade, and lane height.

2.2. Proposed Method

The research begins by collecting remote sensing data and basic road data as the primary dataset. Subsequently, waterlogging points within the study area are gathered to validate the accuracy of the algorithms.

Based on the research data, a dual-layer network assessment model is constructed. In the construction of the model's underlying network, an index system including elevation, rainfall, and other indicators is established. The study area is then uniformly sampled. Using the established index system and a newly proposed method for flood vulnerability assessment, the flood vulnerability indices of all sampling points are evaluated. The city is spatially partitioned using roads as boundaries, and flood vulnerability values for each partition are calculated based on statistics from the sampling points. Each partition corresponds to a node, with the partition's flood vulnerability value as the node weight. All different nodes are interconnected by edges. Finally, differences between partitions are assessed, and the assessment values serve as edge weights. Overall, the underlying network processes the data covered in the index system, establishing a globally coupled network [47]. During this process, the flood vulnerability values of the sampling points reflect the spatial distribution of flood vulnerability within the study area.

In constructing the model's top-level network, three assessments are conducted: based on the underlying network, road disaster vulnerability (RDV) is evaluated. The structural importance of roads is assessed based on the road network structure. Road conditions are assessed based on fundamental road data. Finally, the model integrates the results from the three assessments to determine the road flood vulnerability (RFV). The top-level network utilizes road intersections as nodes and roads as connecting edges. In summary, the top-level network takes inputs from the underlying network and basic road data, producing outputs of road flood vulnerability.

After constructing both network layers, the two can be integrated to form a dual-layer network assessment model. This model enables the assessment of both spatial flood vulnerability and road flood vulnerability in the study area.

The general flowchart of this study is shown in Figure 1.

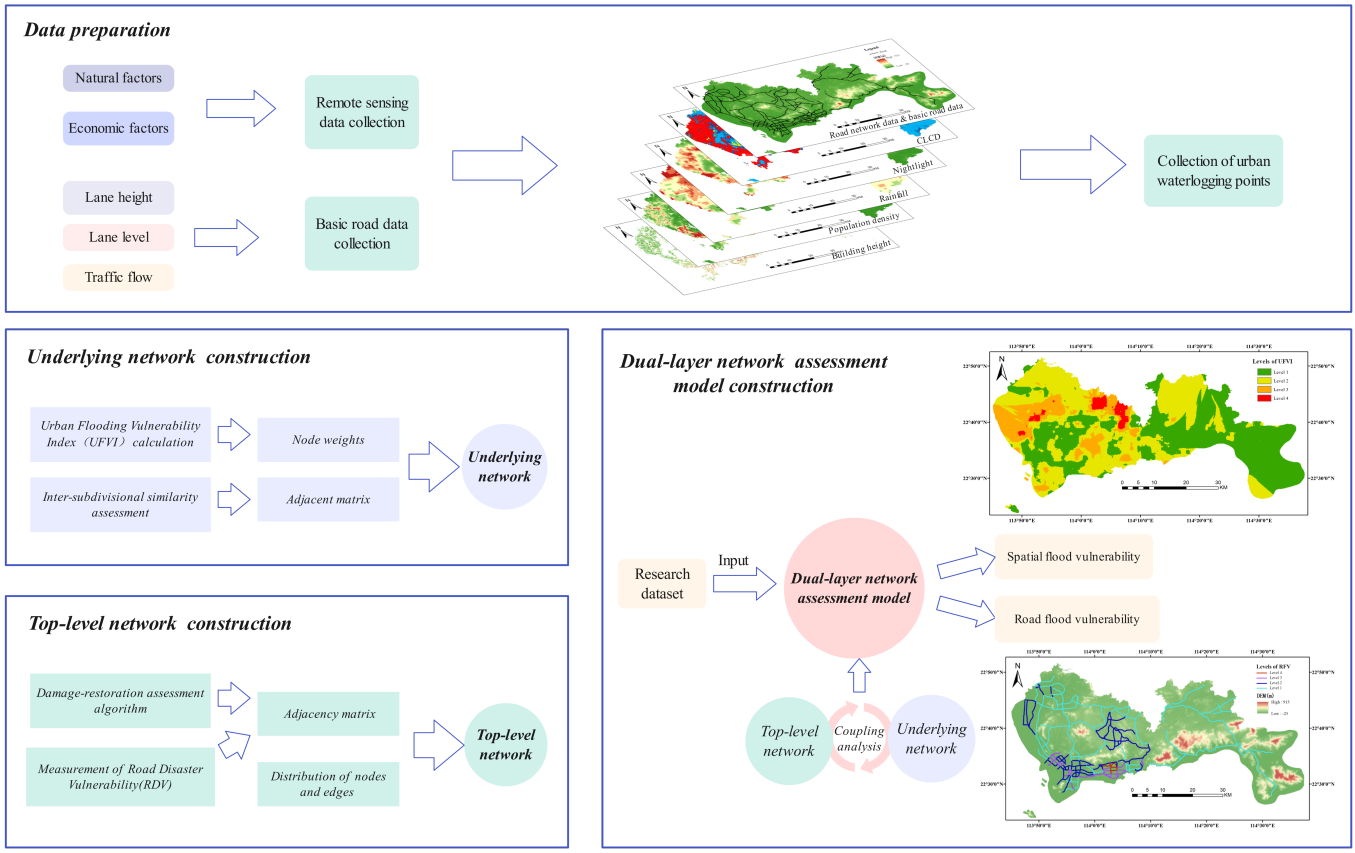


Figure 1. Flowchart of the methodology.

2.3. Underlying Network Construction

This section provides a detailed introduction to the construction process of the underlying network. Section 2.3.1 explains the calculation process of the Urban Flooding Vulnerability Index, which forms the basis for constructing the underlying network. Section 2.3.2 details the calculation of network node weights, and Section 2.3.3 describes the calculation of the network adjacency matrix. Based on the network node weights and the adjacency matrix, the underlying network can be constructed.

2.3.1. Urban Flooding Vulnerability Index (UFVI) Calculation

A new urban flooding vulnerability index (UFVI) is proposed for assessing vulnerability to intra-city flooding. The flowchart of the evaluation algorithm for the UFVI is shown in Figure 2.

The flow of the algorithm's operation is described in detail below.

The indicator system, as the foundation of this algorithm, must be rationally designed at the outset. As this study analyzes flood disaster vulnerability on a small scale, the weak influence of some data that do not change much on a small scale (e.g., education level and emergency preparedness) is ignored. In the construction process of the underlying network, seven types of data are reasonably selected as the study data: elevation data, rainfall data, vegetation distribution data, night light data, population distribution data, building height data, and water body distribution data. Using these data as sources for evaluation criteria, seven evaluation indicators are established. They can be divided into natural and economic categories. Natural indicators include rainfall, elevation, vegetation distribution, and water body distribution. Economic indicators comprise night lighting, population distribution, and building height. These indicators and their interrelationships constitute an indicator system.

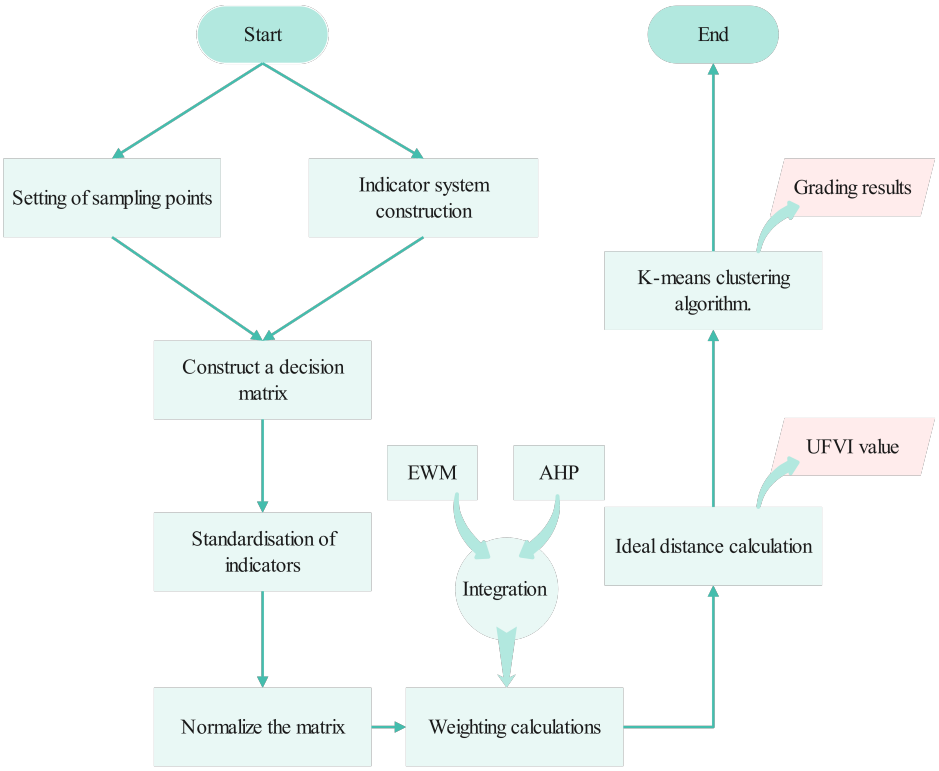


Figure 2. Flowchart of the algorithm for evaluating UFVI values.

The number and values of sampling points affect the algorithm's final assessment outcomes; thus, a rational sampling method needs to be proposed. The algorithm employs a uniform sampling approach, dividing the research area into equally spaced sampling points, and focuses on these points for further analysis. This sampling method overcomes the challenges associated with the fusion of multi-resolution data, preventing the loss of precision that can occur due to data resampling.

After obtaining the sampling points, the following algorithmic process is conducted based on the indicator system.

First, construct a decision matrix. The original matrix X is constructed using m objects and n indexes, where objects represent sampling points, and indexes represent selected indicators.

$$X = (x_{ij})_{m \times n} \tag{1}$$

After that, harmonize the indicator types and perform normalization operations for all indicators. Different indicators represent different meanings. The interval method is used to standardize the indicator values so that they are distributed between 0 and 1.

For the four positive indicators of precipitation, night light, population, and building height, the following normalization operation is applied:

$$x'_{ij} = \frac{x_{ij} - \min(x_{ij})}{\max(x_{ij}) - \min(x_{ij})} \tag{2}$$

For the three negative metrics of elevation, vegetation, and water bodies, the following normalization operation is applied:

$$x'_{ij} = \frac{\max(x_{ij}) - x_{ij}}{\max(x_{ij}) - \min(x_{ij})} \tag{3}$$

In Equations (2) and (3), x_{ij} represents the value at the i-th row and j-th column of matrix X, and x'_{ij} is the data after standardization. Following this step, the original matrix

X needs to be updated. Perform the operation described in Equation (4) on all elements within the matrix X.

$$x_{ij} = x'_{ij} \tag{4}$$

Subsequently, the matrix X needs to be normalized to mitigate the effects of varying magnitudes. The matrix Z obtained after standardizing the indicator values and one element of Z is

$$z_{ij} = \frac{x_{ij}}{\sqrt{\sum_{i=1}^{n} x_{ij}^2}} \tag{5}$$

where z_{ij} represents the element in the i-th row and j-th column of matrix Z. Following Equation (5), Z can be derived, which has dimensions of $m \times n$.

The AHP-EWM method can be used to define the weights among different indicators. The analytic hierarchy process (AHP) [48,49] has a significant advantage over the entropy weight method (EWM) [50,51] in determining weights based on the decision maker's intentions, but it is relatively less objective and more subjective. While EWM offers greater objectivity, it fails to reflect the decision maker's involvement in the importance of different indicators, leading to situations in which certain weights contradict the actual significance of the indicators [52]. To ensure the accuracy and rigor of the assignment, these two types of assignments are combined to seek the weight value of each indicator under each program. This step is roughly divided into the following three small steps:

(1) First, measure weights using the EWM method.

The entropy p_i of the i-th object can be defined as

$$p_i = -k \sum_{j=1}^{m} f_{ij} \ln f_{ij} \tag{6}$$

where $f_{ij} = \frac{z_{ij}}{\sum_{j=1}^{m} z_{ij}}$, $k = \frac{1}{\ln m}$, $i = 1, 2, \ldots, n$. When $f_{ij} = 0$, $f_{ij} \ln f_{ij}$ is defined as 0.

The weight of the i-th object λ_i can be defined according to entropy theory:

$$\lambda_i = \frac{1 - p_i}{n - \sum_{i=1}^{n} p_i} \tag{7}$$

where $0 \leq \lambda_i \leq 1$, and $\sum_{i=1}^{n} \lambda_i = 1$. The vector λ stores the weights of various indicators, as determined by the EWM, featuring dimensions of $1 \times n$.

(2) Then, measure weights using the AHP method.

Initially, establishing a hierarchical framework is imperative. This study considers flood vulnerability assessment as the overarching goal; it encompasses evaluating economic loss and disaster susceptibility as the primary objective.

For each goal, corresponding comparison matrices need to be constructed. The size of the comparison matrix is dependent on the number of indicators to be compared. If the number of indicators is k, then the matrix size will be $k \times k$. In this study, the matrix can be divided into two categories: the criteria layer matrix and the scheme layer matrix. Comparisons between indicators can be quantified using a scale. This evaluation is quantified using a numerical scale from 1 to 9, employing Santy's 1–9 scale for consistent scoring across factors at equivalent levels [53]. The structure of the scale is shown in Table 2. From this, pairwise comparison matrices are developed, synthesizing insights from five specialists in the domain of disasters.

To ascertain the reasonableness of the weight allocation, the following formulas are employed to evaluate matrix consistency:

$$CI = \frac{\beta_{\max} - d}{d - 1} \tag{8}$$

$$CR = \frac{CI}{RI} \tag{9}$$

Table 2. Importance scale used in the AHP method.

Scale	Meaning
1	Equally important
3	Moderately more important
5	Strongly more important
7	Very strongly more important
9	Extremely more important
2, 4, 6, 8	Intermediate values

Herein, $\beta_{\max}$ denotes the principal eigenvalue, d signifies the tally of the criteria, and CI stands for the consistency index. RI represents the mean randomness index, whose value is shown in Table 3. CR, the consistency ratio, serves as a benchmark for coherence; a CR less than 0.1 denotes an acceptable level of consistency.

Table 3. Average randomness index.

Order	1	2	3	4	5	6	7	8	9
RI	0.00	0.00	0.58	0.90	1.12	1.24	1.32	1.41	1.45

The weighted matrix α is calculated using the method described. The matrix α is a 1 by n matrix that stores the weights of each indicator calculated using the AHP method. In this study, both the criteria layer matrix and the scheme layer matrices demonstrate good consistency, affirming the robustness of the methodology. The test results are presented in Table 4.

Table 4. Consistency ratios and indices of different matrices.

Matrix	CR	CI
Criteria Layer Matrix	0	0
Scheme Layer Matrix 1 [1]	1.12×10^{-6}	1.48×10^{6}
Scheme Layer Matrix 2 [2]	4.49×10^{-6}	5.92×10^{6}

[1] Consistency matrix aimed at economic loss. [2] Consistency matrix aimed at disaster susceptibility.

(3) Finally, combine the weights calculated by the two methods.

The weights calculated from both methods are combined to determine the final weights for each category of indicators. We define the subjective and objective combination weights W as follows:

$$w_i = \frac{\sqrt{\lambda_i \alpha_i}}{\sum_{j=1}^{n} \sqrt{\lambda_i \alpha_i}} \tag{10}$$

The matrix W is a 1 by n matrix, where w_i represents the weight of the i-th indicator. After that, W is applied to the matrix Z, which is weighted and averaged for each object to obtain Z:

$$Z = \begin{bmatrix} w_1 z_{11} & w_2 z_{12} & \cdots & w_n z_{1n} \\ w_1 z_{21} & w_2 z_{22} & \cdots & w_n z_{2n} \\ \vdots & \vdots & \ddots & \vdots \\ w_1 z_{m1} & w_2 z_{m2} & \cdots & w_n z_{mn} \end{bmatrix} \tag{11}$$

The element in the i-th row and j-th column of the updated matrix Z is expressed as z_{ij}.

After the calculation of weights is completed, further computations can be carried out based on the principles of the TOPSIS algorithm [54,55]. The positive ideal solution A^+ is

a hypothetical alternative that has the best value for all criteria considered. Conversely, the negative ideal solution A^- represents the worst values. These are defined as follows:

$$A^+ = \{z_1^+, z_2^+, \ldots, z_n^+\}, \text{where } z_j^+ = \{\max(z_{ij}|j \in J), \min(z_{ij}|j \in J')\} \quad (12)$$

$$A^- = \{z_1^-, z_2^-, \ldots, z_n^-\}, \text{where } z_j^- = \{\min(z_{ij}|j \in J), \max(z_{ij}|j \in J')\} \quad (13)$$

where J is related to the positive index, and J' is related to negative indices.

The geometric distances from the ideal solutions are then calculated. S_i^+ is the distance to the positive ideal, and S_i^- is the distance to the negative ideal:

$$S_i^+ = \|z_i - A^+\|_2 = \sqrt{\sum_{j=1}^{n}(z_j^+ - z_{ij})^2} \quad (i = 1, 2, \ldots, m) \quad (14)$$

$$S_i^- = \|z_i - A^-\|_2 = \sqrt{\sum_{j=1}^{n}(z_j^- - z_{ij})^2} \quad (i = 1, 2, \ldots, m) \quad (15)$$

where z_i represents the i-th row of the matrix Z.

The relative closeness of a particular alternative to the ideal solution is given by

$$S_i = \frac{S_i^-}{S_i^+ + S_i^-} \quad (16)$$

Defining the UFVI value as S_i, it is obvious that $0 \leq S_i \leq 1$, and that the larger S_i is, the smaller S_i^+ becomes, meaning that it approaches the maximum value more closely. With this algorithm, the UFVI value for each sampling point can be obtained.

Finally, the K-means clustering algorithm is used to classify the UFVI values for each sampling point. The use of the clustering algorithm for classification is a good choice because of the large number of sampling points used in the study and the uncertainty in the distribution of the resultant data from different study areas [56,57]. In this study, the K-means clustering algorithm is selected for UFVI classification to indicate the risk level of flooding.

With this algorithm, the UFVI is categorized into four levels (levels 1 to 4), with higher levels indicating a higher severity of vulnerability. Using this algorithm, the UFVI level at each sampling point can be determined efficiently.

2.3.2. Node Weight Calculation

To study the flood vulnerability of roads more intuitively, our study utilized road network vector data to delineate the study area, with roads as boundaries. The areas enclosed by the road network are defined as blocks, and each block is considered a node of the underlying network. Using the UFVI values within each area, the proposed algorithm is employed to statistically assess the flood vulnerability of each block. The flowchart of this process is illustrated in Figure 3.

The algorithm is briefly explained below. Intersections are first extracted from the road network, and the partitioning boundaries are defined based on the rectangular area formed by the maximum and minimum latitude and longitude values of the four intersections. To facilitate computer operations, this latitude and longitude range is taken as the physical range of the partition, and the appropriate latitude and longitude spacing are used for sampling the area. Finally, the average of the sampling results is used as the weight of the node corresponding to the partition. Utilizing this algorithm, the flood vulnerability value of each partition can be evaluated to obtain the node weights of the underlying network.

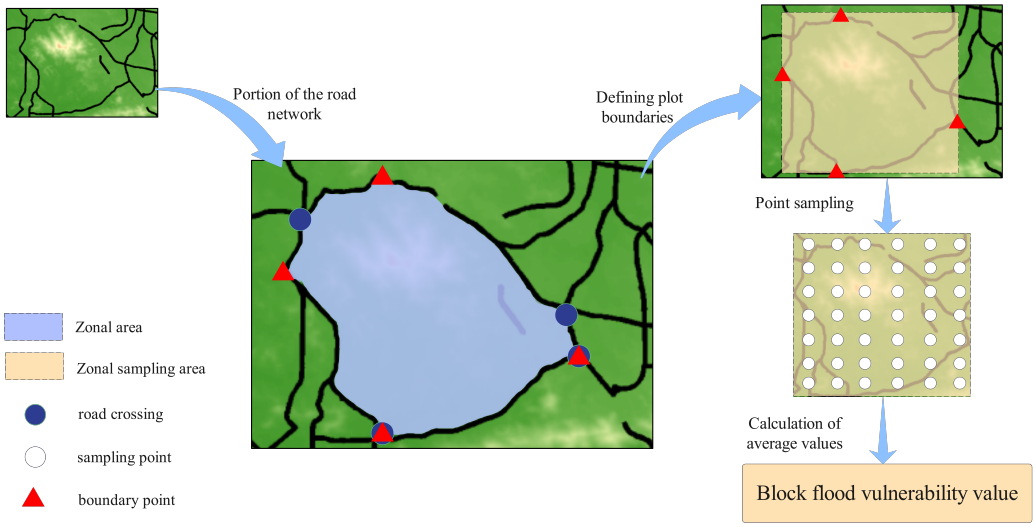


Figure 3. Flowchart of the partition vulnerability assessment algorithm.

2.3.3. Adjacent Matrix of the Network

The weights of the edges represent the degree of similarity in flood vulnerability of neighboring regions. The distance between two regions is the main determinant for assessing the degree of similarity in flood vulnerability [58]. In addition to physical distance, some static features should be considered in combination.

Seven static features, such as height and rainfall, are chosen for similarity comparison, as shown in Table 5. Using Euclidean distance to analyze the similarity of indicators in different regions, the static feature similarity indicator H is obtained. Defining the node weights of the underlying network as UW, the physical distance as D, the weight of the physical distance as a, and the similarity weight as b, Equation (17) is obtained as follows:

$$\mathrm{UW} = a \cdot D + b \cdot H \tag{17}$$

where a and b are variable parameters, which are reasonably assigned based on different study areas to ensure that they can reasonably reflect the differences in flood risk between the two regions.

2.4. Top-Level Network Construction

Based on the road network vector data, the basic structure of the top-level network can be constructed. The flood vulnerability values of roads, used as the weights of edges, need to be appropriately assessed. To determine the flood vulnerability values of roads (i.e., edge weights), our research is structured into three dimensions. Section 2.4.1 assesses the disaster vulnerability of roads, Section 2.4.2 evaluates their relative importance within the network structure, and Section 2.4.3 examines the roads' capacity for disaster bearing and resilience as part of the transportation system. Finally, the results from these assessments are integrated in Section 2.4.4 to derive the roads' flood vulnerability values.

2.4.1. Road Disaster Vulnerability Analysis

Road vulnerability is primarily related to the degree of flood vulnerability in surrounding areas, which can be measured using the UFVI values. Based on this, the concept of similarity is introduced. If there is a high degree of similarity between the areas on both sides, the spread of hazard vulnerability from one side to the other is often small, and the impact on the road is small; conversely, the impact is often large [59]. The degree of similarity of flood vulnerability between different areas is obtained from the adjacent matrix of the underlying network. To better quantify the vulnerability of roads, the following

formula is proposed for calculating road disaster vulnerability (RDV) based on the degree of vulnerability:

$$RDV = (L_{\max} - L_{\text{avg}}) \times R + L_{\text{avg}} \tag{18}$$

where $L_{\text{avg}} = (\gamma + \beta)/2$, $L_{\max} = \max(\gamma, \beta)$, γ and β represent the node weights of the two districts connected by the road in the underlying network, and R represents the edge weight between these nodes.

RDV is the most important indicator for assessing roadway flood vulnerability (RFV), which marks the degree of susceptibility of a roadway to flooding.

2.4.2. Analysis of the Structural Significance of Roads

In transportation systems, the robustness of the traffic network is a critical characteristic for maintaining network functionality under various stresses and impacts [60]. Robustness refers to the ability of a network to continue its core operations amidst external disruptions or internal failures [27,61]. Following flood disasters, various routes inevitably become non-functional, leading to their disconnection from the traffic network [62]. In such scenarios, assessing the robustness of the remaining traffic network after road disconnections can reveal the significant impact of those roads on the overall network. In this paper, this impact is defined as the structural significance of the road.

To assess the structural significance of roads, it is necessary to model the road network of the study area. Initially, we abstract the road network structure into a complex network, G, where road intersections serve as network nodes and the roads themselves as the edges.

Subsequently, a method is proposed to assess the robustness of the traffic network, focusing on two aspects: connectivity and redundancy. Connectivity refers to the capacity to establish links between nodes within a transportation network, and is closely related to the robustness of the transportation network [63]. It is crucial for enhancing transportation system accessibility as it directly affects how easily different areas can be reached via road networks [64]. A highly connected traffic network can maintain operational efficiency even when some routes are closed [65]. Redundancy refers to the presence of extra or backup routes in the traffic network, which can be utilized when primary routes are unavailable [66]. This redundancy provides the network with greater flexibility and stability in the face of localized failures [67]. A connectivity efficiency evaluation algorithm based on the K-shortest paths algorithm is proposed, which comprehensively considers both connectivity and redundancy. A detailed description of this algorithm is provided below.

Yen's K-shortest paths algorithm, based on Dijkstra's algorithm, calculates the k-th-shortest path between every pair of distinct nodes [68]. Utilizing this algorithm, one can collect the lengths of the first k-shortest paths between every two nodes. The pseudo-code of the algorithm is shown below (Algorithm 1).

Assuming the shortest distance between two points is dt_1, the second-shortest distance is dt_2, and the third-shortest distance is dt_3. Let m be the number of reachable paths between two points. The longest distance between any two points in the entire graph is defined as $dt_{\max}$. Considering the driving preferences in the transportation system [69,70], Equation (19) can be proposed.

$$p = \begin{cases} 0.75 \cdot dt_1 + 0.2 \cdot dt_2 + 0.05 \cdot dt_3, & \text{if } m \geq 3 \\ 0.75 \cdot dt_1 + 0.25 \cdot dt_2, & \text{if } m = 2 \\ 1.5 \cdot dt_1, & \text{if } m = 1 \\ dt_{\max}, & \text{if } m = 0 \end{cases} \tag{19}$$

In Equation (19), if there are fewer than three alternative routes, the distance between two points will be longer compared to paths with more alternatives. This calculation method can be seen as a penalty mechanism for low network redundancy, as low redundancy is often associated with low robustness [67]. Based on Algorithm 1 and Equation (19),

the distance measurement indicator p between any two distinct nodes in the traffic network can be assessed.

Algorithm 1 Yen's K-Shortest Paths Algorithm

Require: A graph G with vertices V and edges E represented as adjacency list, source vertex s, and target vertex t.

```
Initialize list A to contain the shortest path from s to t using Dijkstra's algorithm.
Initialize a priority queue B to store potential k shortest paths.
for k = 1 to K do
    Let p be the last path in A.
    for each vertex v in p except t do
        Spur node u is v.
        Spur path is from s to u in p.
        Remove all links from G that are part of the paths in A that share the same spur path up to u.
        Temporarily remove all nodes in p up to u except u itself.
        Use Dijkstra's algorithm to find a spur path from u to t.
        if a spur path is found then
            Total path is the combination of the spur path and the initial part of p.
            Add the total path to B if it is not already in A or B.
        end if
        Restore edges and nodes to G.
    end for
    if B is empty then
        break
    end if
    Add the shortest path from B to A.
    Remove this path from B.
end for
return A.
```

Ensure: The k shortest paths from s to t are stored in list A.

The transportation network not only has transportation characteristics but also exhibits the traits of a small-world network [71]. Latora et al. proposed an evaluation scheme for the efficiency of small-world networks [72]. They defined the global efficiency of a network G as the average of the inverse of the shortest path lengths between all distinct nodes. Considering that the primary purpose of the transportation system is to perform transportation tasks, it may experience congested traffic conditions [73]. In congested traffic networks, users often choose multiple alternative routes as travel plans [74]. Additionally, the redundancy of the transportation network plays an important role in disaster resilience [75]. Taking these practical factors into account, p from Equation (19) is used as the metric for measuring the distance between two points. This leads us to propose a new scheme for evaluating the efficiency of transportation networks, E, as shown in Equation (20).

$$E = \frac{1}{N \cdot (N-1)} \cdot \sum_{i=0}^{N} \sum_{\substack{j=0 \\ j \neq i}}^{N} \frac{1}{p_{ij}} \tag{20}$$

where N represents the number of nodes in G. p_{ij} represents the p value between points i and j, where i and j denote the node numbers.

Finally, we apply the Damage and Recovery Assessment Algorithm (DRAA) to network G. To evaluate the structural significance of roads, we develop the DRAA, which sequentially disconnects each road and observes the resultant changes in the global road network efficiency. This process helps identify the criticality of each road within the network structure. The pseudocode for this algorithm is shown below (Algorithm 2).

Algorithm 2 Damage and Recovery Assessment Algorithm

Require: Road network vector data.

Read the road network structure with N edges.
Calculate the average efficiency (E_0) of the entire map.
$n \leftarrow 0$
while $n < N$ **do**
    Disconnect the edge numbered n from the graph.
    Recalculate and save the average efficiency of the new network (E_n).
    Reset the graph to its original state, $n \leftarrow n + 1$.
end while
Normalize the list E.
Save the list E.

Ensure: Evaluation value of the structural importance of each road.

By employing this algorithm, the structural significance values of each road are compiled into a list. This analysis facilitates the identification of road sections that have the potential to significantly disrupt the network's structural integrity.

2.4.3. Assessing Roads' Disaster-Bearing Capabilities from Road Conditions

In addition to the structural importance of the transportation network and road disaster vulnerability, the construction conditions and the development level of the lanes are also factors that determine the vulnerability of roads to flooding. The traffic volume V_t is selected to measure the level of road development. Lane width W, lane height H, and lane grade R are three indicators selected to measure lane resistance to damage. The more developed the road, the greater the economic loss because of flood damage and the higher the road's flood vulnerability. The stronger the road's ability to resist damage, the better its protective performance and the lower its vulnerability to flooding.

The opinions of three experts in the transportation field have been obtained, and the AHP method has been used to measure the weights from two aspects: physical damage and functional impairment of the road. After the indicators are normalized, the following weight allocation is used to calculate the road's inherent vulnerability θ:

$$\theta = 0.71598 \cdot V_t - 0.14949 \cdot H - 0.6849 \cdot R \tag{21}$$

2.4.4. Calculation of Overall Road Flood Vulnerability

With the aforementioned methods, the values of RDV, E, and θ can be obtained. The road flood vulnerability results can be determined using these values. The opinions of five disaster domain experts have been sought, and the AHP method has been applied to calculate weights from three aspects, namely, disaster resilience, economic loss because of disasters, and social impact, thereby obtaining the weight values. Road flood vulnerability (RFV) can be measured using Equation (22):

$$RFV_i = 0.76924 \times RDV_i + 0.14676 \times E_i + 0.084 \times \theta_i \tag{22}$$

where i is in the range [0–t], and t represents the total number of road segments.

The RFV of roads is used as the weights of the edges corresponding to roads in the top-level network. Based on the road network structure, the top-level network can be constructed.

3. Experiment

This section introduces the experimental setup information and details. Section 3.1 provides further information about the study area. Section 3.2 describes the experimental preprocessing information, Section 3.3 outlines the construction process of Shenzhen's dual-layer evaluation network, and Section 3.4 presents the flood vulnerability assessment results for Shenzhen and provides an analysis.

3.1. Study Area

In this study, Shenzhen City is used as the study area for the experiment, as shown in Figure 4. Shenzhen is located in the southern region of Guangdong Province, China, on the east coast of the Pearl River Delta [76]. Flooding and storm surges are frequent because of its coastal mountainous terrain and frequent typhoons at low latitudes [77–79]. Floods have caused great economic losses and extensive impacts in Shenzhen [80]. In Figure 4, the Digital Elevation Model (DEM) illustrates the variations in elevation across the area.

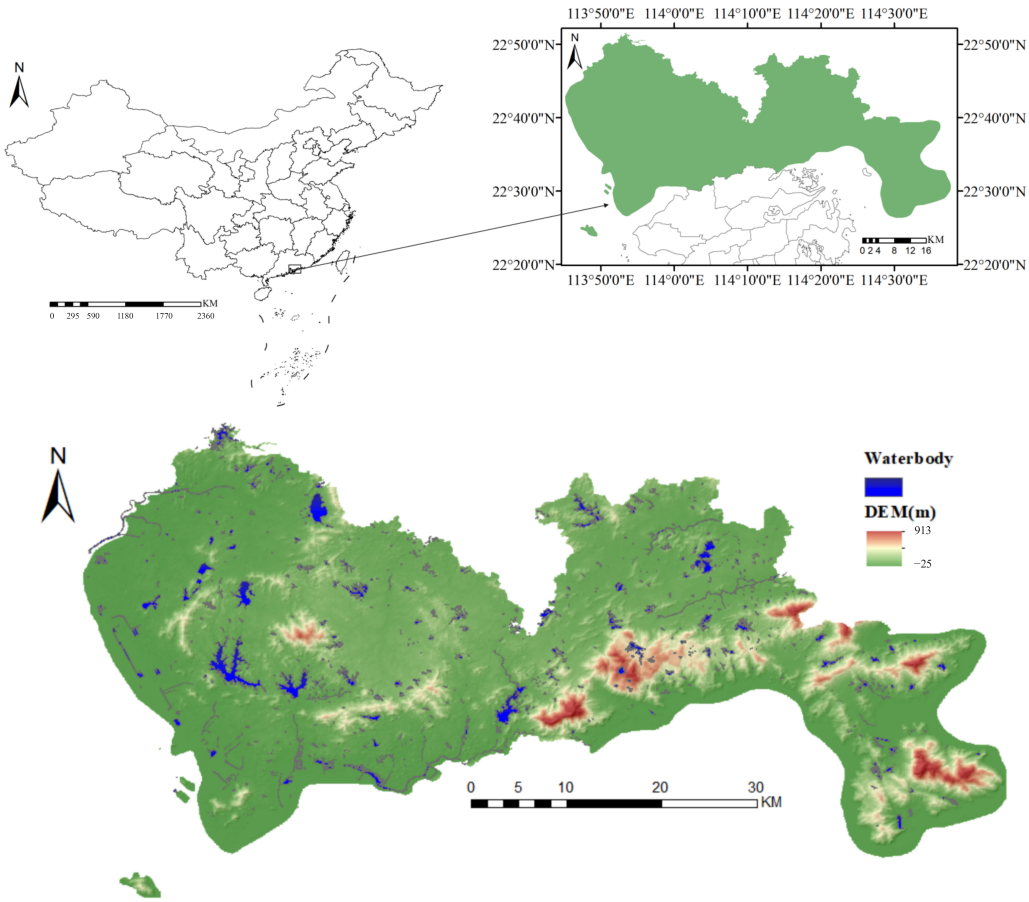


Figure 4. Location and elevation maps of the study area.

3.2. Experimental Setup

This section provides a detailed explanation of the data used in the experiment and describes the preprocessing operations conducted.

3.2.1. Underlying Network Data Interpretation

In the construction of the underlying network, seven types of data are selected to constitute seven types of indicators. These indicators are categorized into two main types: economic and natural. Economic indicators reflect the socioeconomic status of the study area, covering aspects such as night lighting and population distribution. Natural indicators, on the other hand, reveal the physical geography of the region, including factors such as rainfall and elevation. The indicators are explained for ease of understanding. The interpretations of these indicators are provided in Table 5.

In the indicator system, the vegetation distribution indicator is measured based on the shortest distance from the sampling point to areas covered by vegetation, and the water body distribution indicator is assessed based on the shortest distance from the sampling point to water bodies. The units for both indicators are meters. The night lighting indicator

is derived from the average visible band digital number (DN) of cloud-free light detections multiplied by the percent frequency of light detection. The indicators in Table 5 and their corresponding units are shown in Table 6.

Table 5. Urban flooding vulnerability assessment indicator system.

Category	Indicator	Properties	Indicator Meaning
Nature	Rainfall	Positive	Rainfall is an important cause of flood and waterlogging disasters, so considering it an important indicator in the assessment is necessary [81].
	Elevation	Negative	Altitude affects the pressure in urban storm-water systems; low-lying areas are more vulnerable to rain and flood damage [82,83].
	Vegetation distribution	Negative	Vegetation has water storage capacity and certain flood and waterlogging disaster resistance.
	Water body distribution	Negative	The closer a region is to rivers and lakes, the greater the possibility of flood inundation [84].
Economic	Night lighting	Positive	The higher the night light value and the more vibrant the economy, the greater the losses resulting from flood and waterlogging disasters [85,86].
	Population distribution	Positive	The most direct impact of floods is on the urban population [19]. The greater the population density, the greater the damage caused by flood and waterlogging disasters.
	Building height	Positive	Urban buildings are the main bearers of waterlogging [19]. The taller the buildings and the more developed the economy, the higher the losses caused by flood and waterlogging disasters.

Table 6. Indicators and their corresponding units.

Indicator	Rainfall	Elevation	Vegetation	Water Body	Night Lighting	Population	Building Height
Unit	mm/year	m	m	m	/	people/km^2	m

3.2.2. Top-Level Network Data Interpretation

During the construction of the top-level network, some data are selected for the construction and analysis of the network. These data have a high correlation with the flood vulnerability of roads. For ease of understanding, the interpretation of these data is shown in Table 7.

Table 7. Explanation of the data related to the top-level network.

Data Name	Explanation
Road Network	The structure of the road network determines the structural importance of roads [87]. Structural importance can be analyzed through road network data.
Traffic Volume	This reflects the number of vehicles passing on a road unit over time [88]. A higher traffic volume implies greater damage to the road and higher subsequent losses. In this experiment, the traffic volume of the roads is measured on an annual basis.
Lane Grade	This is related to urban planning, in which different grades correspond to different construction standards. Higher grades imply greater safety and stronger resistance to damage.
Lane Elevation	This is basic information about a road. Higher lanes have a lower water retention capacity and stronger flood resistance.

3.2.3. Data Preprocessing

All datasets are projected using the WGS_1984_UTM_ZONE_50N coordinate system to ensure accuracy in overlay computations and to avoid potential errors.

Because of the existence of small differences in the coverage of different types of data, there are missing values for a few categories in a very small number of areas. To address

this issue, the proximity principle is applied, substituting the missing values with the average values from adjacent areas to minimize the errors resulting from data gaps.

3.3. Network Construction and Analysis

This section, following the order of model construction, takes Shenzhen City as the research area and describes the construction processes of the underlying network, the top-level network, and the network integration process for the dual-assessment network of Shenzhen City. Necessary explanations and analyses of the construction results are also provided while introducing the construction processes.

3.3.1. Underlying Network Construction and Analysis

- UFVI calculation and analysis.

First, Shenzhen is sampled with 2952 sampling points selected. Based on the indicator system, the weights for all sampling points can be calculated using Equations (6)–(10). The weighting results are shown in Table 8.

Table 8. Weighting results.

Index	Weight
Vegetation	0.125197903
Building Height	0.137840032
Population	0.124066944
Water Body	0.246290453
Rainfall	0.151109107
Elevation	0.115716417
Nightlight	0.099779145

After the weights are calculated, the UFVI of waterlogging in Shenzhen is analyzed. The UFVI values for each sampling point are calculated using Equations (11)–(16). The maximum value of the index is 0.67155, and the minimum value is 0.03902, with a relatively discrete distribution.

According to our method, based on the K-means clustering algorithm, Shenzhen City is subsequently categorized into four levels of UFVI: level 1 (0.03902–0.19062), level 2 (0.19117–0.27015), level 3 (0.27043–0.38704), and level 4 (0.39002–0.67155). Specifically, 56.045% of the areas fall into level 1, indicating low vulnerability to flooding. Level 2 vulnerable areas constitute 28.310%, level 3 areas make up 13.241%, and level 4 areas, the most vulnerable, account for 2.404% of the total area. This distribution reveals that the majority of Shenzhen exhibits relatively low susceptibility to flood hazards, indicating that the flood risk is generally manageable across the region. Nevertheless, a notable proportion of the city is at a higher risk of flooding, underscoring the importance of targeted mitigation and preparedness strategies.

- Node weight calculation and analysis.

Shenzhen City has multilevel roads, and for simplicity of the research process, the first-level roads in Shenzhen City are selected as the research object. Taking the road network as the partition boundary, Shenzhen is divided into 82 small partitions, and the average UFVI value of each partition is obtained using the uniform sampling method to obtain the flood vulnerability results of each partition. The UFVI average of each partition is used as the node weight.

Figure 5 depicts the spatial distribution of vulnerability across the districts of Shenzhen. In Figure 5, the nodes denote the positions of different districts, concurrently symbolizing the nodes of the underlying network. Nodes in red signify districts whose flood vulnerability index ranks in the top 20%, indicating these areas are at a heightened risk level. The red dashed lines in the figure delineate the concentrated distribution of high-vulnerability zones. Notably, areas with heightened risk predominantly cluster in the southwestern part

of Shenzhen, while eastern regions exhibit comparatively lower flood vulnerability, and thus, demonstrate a clear geographical distribution trend. This distribution trend may be related to the higher terrain and less economic activity in the east.

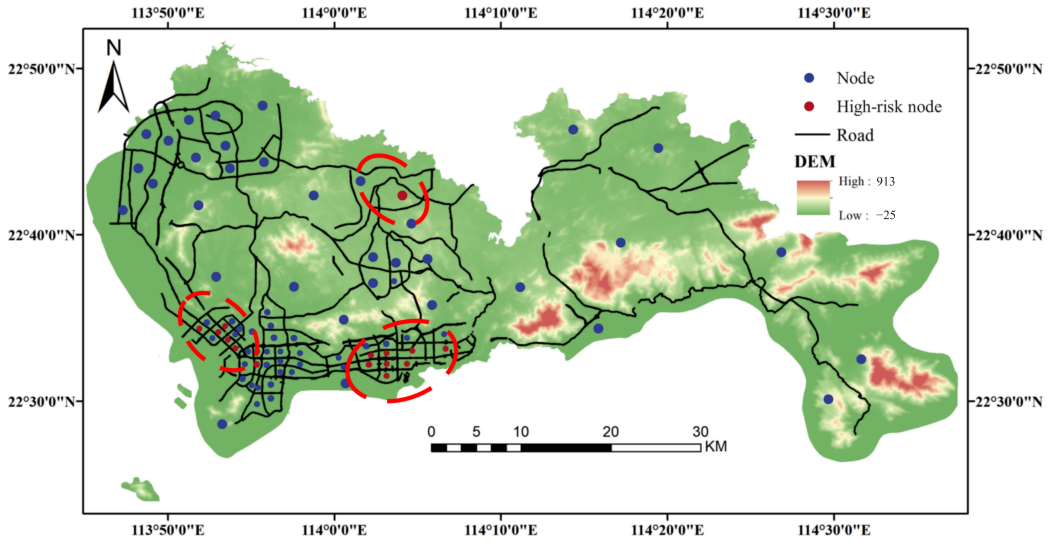


Figure 5. Road network and zoning schematic.

It is particularly striking that those areas with higher risks are largely located in the urban core, underscoring their pivotal role in the city's structure and economic activities. However, this also implies that, in the event of a flood disaster, these densely populated commercial hubs, critical infrastructure, and important cultural heritage sites could suffer severe impacts. Consequently, rational protection and preventive measures for these key areas are of the utmost importance. Not only can such measures mitigate potential economic losses, but they can also play a crucial role in safeguarding the lives and property of urban residents. The precise identification and assessment of these high-risk areas provide vital decision support for urban flood management. In turn, this enables the implementation of more effective flood mitigation and reduction strategies and enhances the city's resilience and recovery capacity in the face of disasters.

- Adjacent matrix of the network.

In this study, based on the specific situation of Shenzhen, for Equation (17), we choose 0.7 as the weight value of physical distance and 0.3 as the weight value of similarity. By assessing the interval similarity among 82 districts, the edge weights of Shenzhen's underlying complex network are obtained. The distribution of the underlying edge weights in Shenzhen is relatively dispersed. Specifically, nodes that are physically adjacent tend to have lower edge weights. This aligns with the algorithmic process of similarity assessment.

Upon obtaining the adjacency matrix, and combining the nodes and their weights, the underlying network for the study can ultimately be constructed.

3.3.2. Top-Level Network Construction and Analysis

Based on the delineation of districts, the road network in Shenzhen City is divided into 178 segments. From Equation (18), the road hazard vulnerability can be calculated for each road section.

The RDV value serves as the primary indicator for assessing the flood vulnerability of roads, representing the likelihood of flood disaster occurrence on a given road segment. Its distribution is relatively concentrated, with distribution patterns as shown in Figure 6a. This indicates that on the small scale of Shenzhen City there is minimal variation in disaster susceptibility. Roads such as Hongli Road, Caitian Road, and Xinzhou Road exhibit higher flood vulnerability. These roads are close to water sources, are located in economically

developed areas, have high disaster vulnerability and economic damage potential, and need to be reasonably protected.

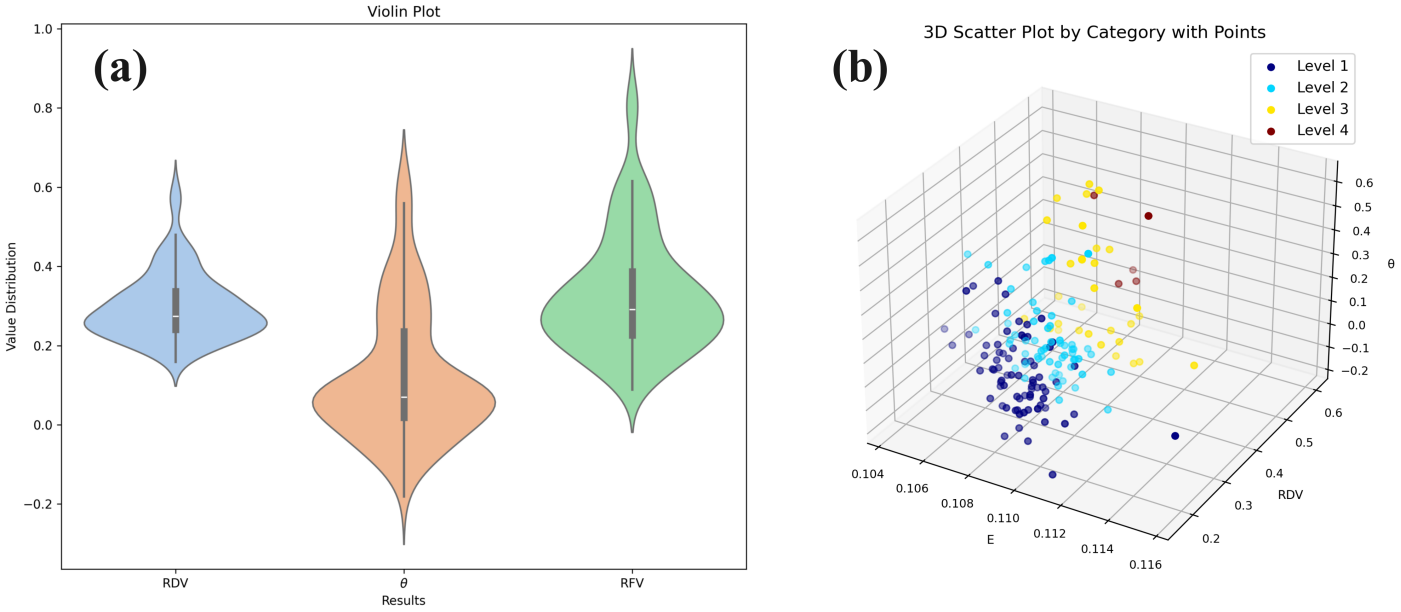


Figure 6. (**a**) Violin plot of the results; (**b**) 3D scatter plot by category with points.

Subsequently, based on the vector data of the road network, the structural significance of each road is analyzed from the perspective of transportation network robustness. The distribution of structural significance values among different roads is relatively concentrated. Roads such as Xiangmihu Road, Shennan Boulevard, and Yanhebei Road have higher structural significance. These roads, mostly located in Shenzhen's central areas, play critical roles in linking the network tightly. Disruptions to these roads could have a substantial impact on the overall efficiency of the road network.

Further analysis of road conditions sheds light on the disaster-bearing capacity of roads. This distribution is also dispersed, as depicted in Figure 6a, with roads such as Huiyan Middle Road and Yanlong Avenue exhibiting high inherent vulnerability. Factors such as road elevation, construction conditions, and traffic volume contribute to a road's inherent vulnerability.

Combining the above results, the roadway flood vulnerability (RFV) can be assessed. The trend in RFV index distribution is shown in Figure 6a. The distribution of the RFV index is relatively discrete, which can effectively reflect the differences in road vulnerability. To facilitate the analysis, the clustering algorithm is used to hierarchize the index, which is divided into level 1 vulnerable roads (0.020667–0.267439), level 2 vulnerable roads (0.271379–0.430134), level 3 vulnerable roads (0.441443–0.641757), and level 4 vulnerable roads (0.750865–0.842680). The schematic of the clustering classification is shown in Figure 6b. The risk level of roads in Shenzhen City is generally stable, but some roads have a higher risk. After the RFV value is calculated, the construction of the top-level network can be completed based on the road network structure.

3.3.3. Dual-Layer Network Construction

A dual-layer assessment network for Shenzhen City can be constructed by integrating the underlying network with the top-level one. The top-level network is a road network with intersections as nodes, and its edge weights are determined by the node weights and edge values of the underlying network. To facilitate understanding, the dual-layer network structure is illustrated using a small section of Shenzhen City, as shown in Figure 7. Utilizing this network model allows for the analysis and determination of road vulnerability in a comprehensive and detailed manner.

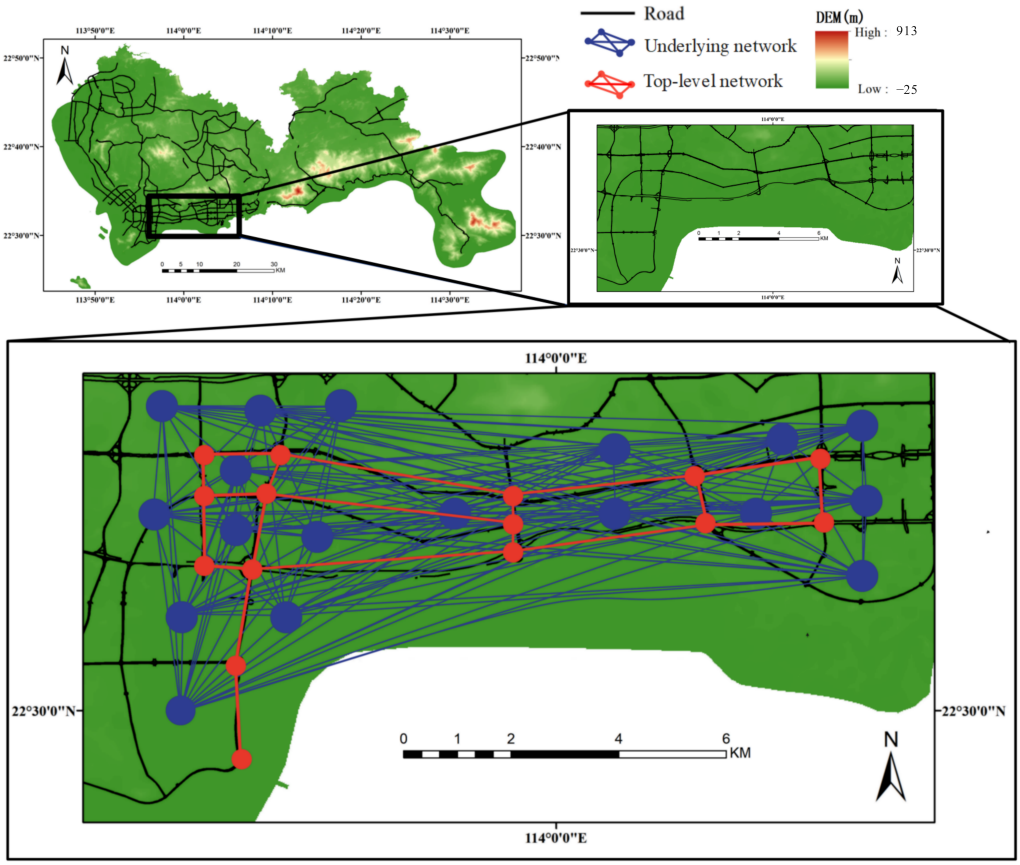


Figure 7. Dual-layer assessment network diagram.

3.4. Experimental Results

This section presents the spatial vulnerability assessment results for Shenzhen City obtained from the evaluation model, as well as the road vulnerability assessment outcomes, and provides an analysis of the results.

3.4.1. Analysis of Spatial Flood Vulnerability in Shenzhen

Using the results of the dual-layer assessment network, this study obtains the flood vulnerability results for the space of Shenzhen City, as shown in Figure 8.

The spatial distribution characteristics of flood vulnerability in Shenzhen reflect the geographical differences in the city's susceptibility and responsiveness to floods. Flood vulnerability in Shenzhen shows a specific spatial distribution pattern, mainly concentrated in the northern and western regions, forming a gradient of vulnerability that gradually decreases from west to east. Specifically, the eastern regions, especially those near mountainous zones, exhibit relatively low flood vulnerability because of their higher elevation and rich vegetation cover, and they are mainly categorized as level 1 and level 2 vulnerability areas. The natural conditions in these areas are conducive to rainwater absorption and drainage, thereby reducing the potential for flooding. By contrast, the southern and northwestern areas of Shenzhen have higher vulnerability indices because of their high levels of economic development, rapid urbanization, high population density, and low topography, suggesting that these areas have higher risks and loss potential in the face of flooding. In particular, Nanshan District, Futian District, and Luohu District, which are the economic and administrative centers of Shenzhen, are not only densely populated but also have frequent commercial activities and intensive infrastructure construction, which may lead to significant economic losses and social impacts in the event of flooding. This situation suggests that urban planning and flood control measures need to fully consider the special vulnerability of these areas.

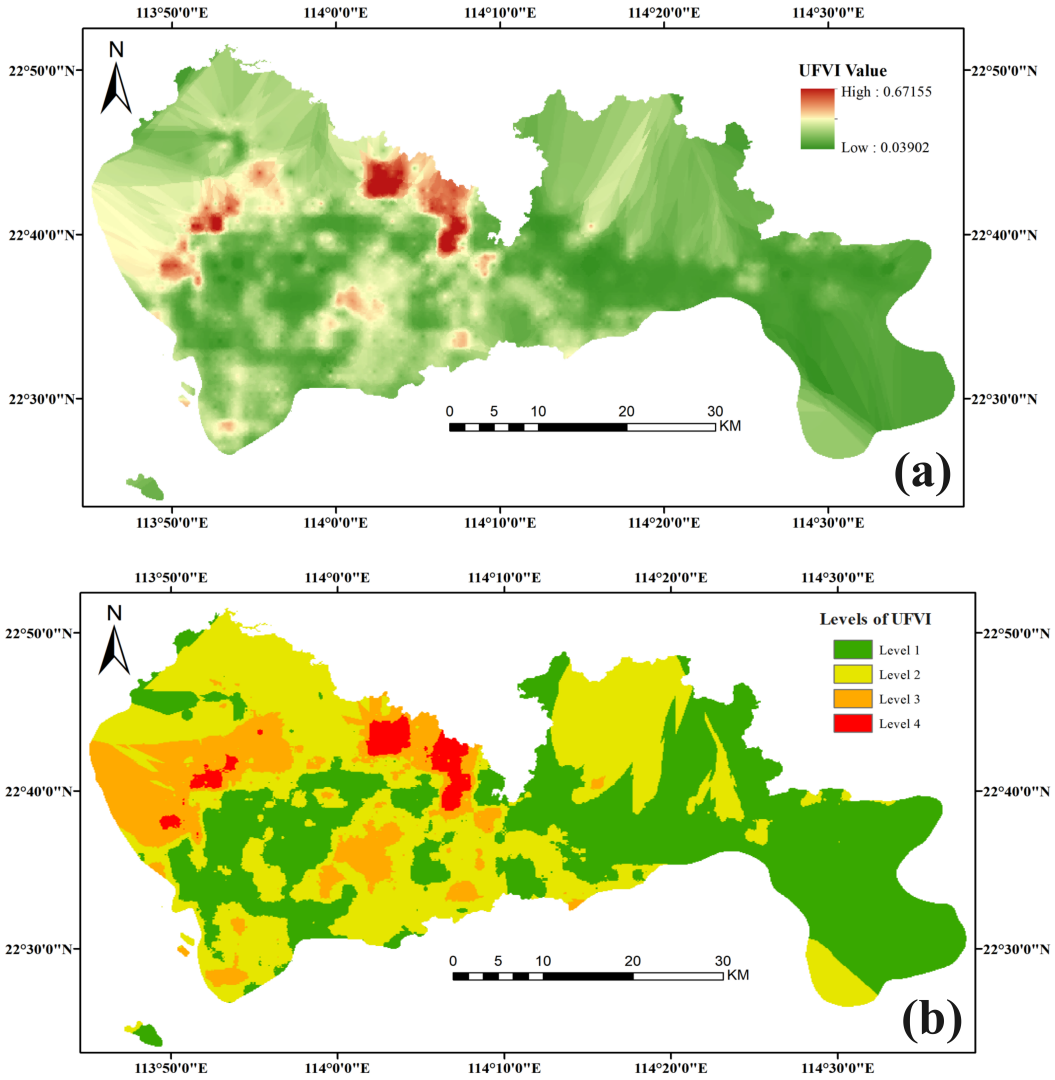


Figure 8. (**a**) Trends in the distribution of UFVI values; (**b**) map of flood vulnerability classification.

3.4.2. Analysis of Roadway Flood Vulnerability in Shenzhen City

Utilizing the outcomes from the dual-layer assessment network, this study delineates the flood vulnerability of the roads under examination, as depicted in Figure 9.

Notably, roads with elevated flood vulnerability predominantly cluster in Shenzhen's southwestern segment. These zones, situated within Shenzhen's urban core, boast robust economic frameworks and exhibit lower elevations. Consequently, there is substantial reliance on road usage in these areas, highlighting their susceptibility to significant flood risks and potential losses. In addressing urban development and flood mitigation, the maintenance and repair of these roads must be prioritized to increase the city's resilience to the threat of flooding. Roads characterized by low flood vulnerability are primarily found in the eastern sectors of the city, where higher elevations, lower population densities, and reduced vehicular flow contribute to their lower susceptibility to flooding.

In Shenzhen's road network, certain road sections exhibit high RFV scores. The details of the top ten roads in Shenzhen based on their RFV scores are shown in Table 9. These roads have a high vulnerability to flooding compared to other roads, and they are in the higher-risk range of flooding and need to be protected by the relevant authorities.

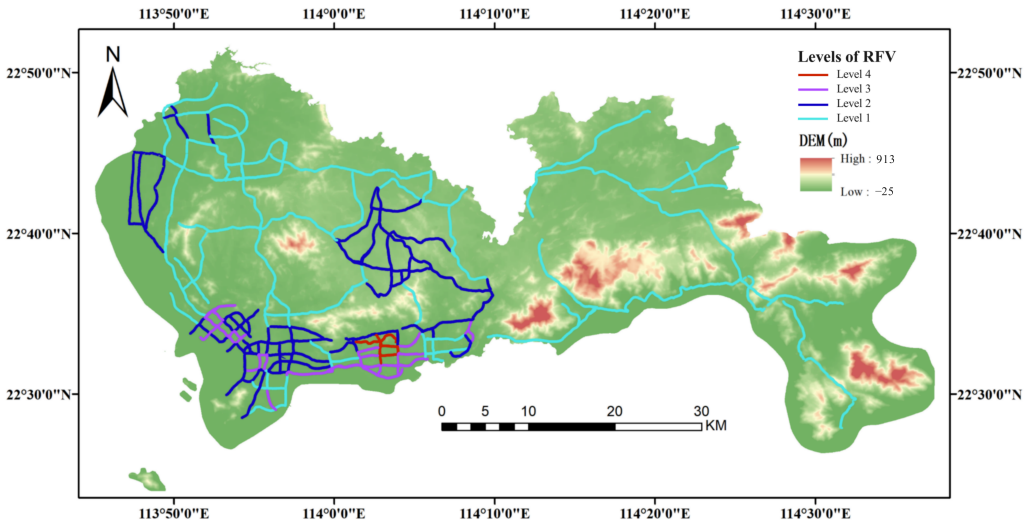


Figure 9. Road flood vulnerability classification map.

Table 9. Level 4 flood vulnerability road information.

Road ID	Road Name	RFV Value	Road ID	Road Name	RFV Value
100	Caitian Road South Section	0.59785	108	Hongli Road West Section	0.60161
111	Xiangmi Lake Road	0.60853	110	Shennan Avenue West Section	0.61369
33	Guangshen Road	0.61562	172	Baoan Avenue	0.64177
106	Xinzhou Road North Section	0.75087	98	Caitian Road North Section	0.80870
101	Shennan Avenue East Section	0.81012	104	Hongli Road Middle Section	0.84268

4. Discussion

This section discusses the research methodology and findings of the study. Section 4.1 presents the validation of flood points in the assessment of urban spatial flood vulnerability. Section 4.2 compares the research method of this study with those of related studies, indicating that our methodology addresses research gaps. Section 4.3 offers recommendations, based on the assessment results, for the prevention of flood disasters.

4.1. Waterlogging Point Verification

In recent years, Shenzhen has been affected by catastrophic weather events, particularly urban flooding caused by sudden heavy rainfall, which has become increasingly severe. Numerous roads throughout the city have been disrupted because of waterlogging, with frequent occurrences of flooded areas. This study has compiled data from 2019 to 2023, identifying 54 waterlogging points. These data are primarily based on government reports, field investigations, and news reports. The distribution of these waterlogging points is shown in Figure 10.

As can be seen from the figure, the distribution of these waterlogged points is roughly similar to the distribution pattern of flood vulnerability, which indicates that our findings are scientifically sound. From the reports of waterlogged points released by the relevant departments, they are mainly concentrated in the southwestern part of the city, and most of these areas are in level 2 or higher vulnerability zones, which is consistent with the results of our analysis. However, waterlogged points are not representative of flood vulnerability. Some of the waterlogged points may occur because of building construction, aging of the drainage network, and other factors. Therefore, there are still some waterlogged points that are in level 1 vulnerability zones. Overall, our research findings are consistent with the distribution patterns of waterlogged points and possess a high degree of credibility.

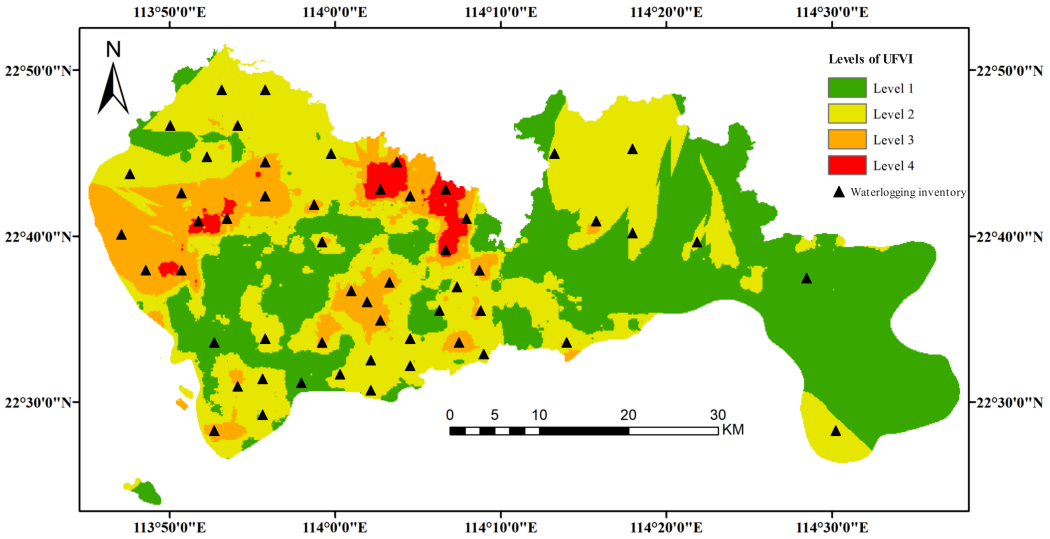


Figure 10. Waterlogging point verification map.

4.2. Comparison with Other Evaluation Methods

To evaluate the validity and accuracy of the methodologies used for assessing road vulnerability to flooding, the methods are compared with those from similar studies.

With the advent of remote sensing technology, an increasing number of researchers are exploring disaster vulnerability based on remote sensing data [89,90]. Different researchers have used different research tools for flood vulnerability assessment. Those articles that use the complex network approach to evaluate road vulnerability typically analyze the vulnerability of roads solely in terms of network structure. For example, Refs. [6,31] examined road vulnerability from the perspective of road network structure, whereas Refs. [30,91] investigated the disaster resilience of streets based on their intrinsic characteristics. Other researchers studied hazards themselves from the perspective of mathematical modeling, often ignoring the network structures of roads. For instance, refs. [5,92] did not consider the significance of the road network structure to roads. These studies provide good recommendations for flood vulnerability assessment methods, but they tend to ignore the complex relationship between the road network structure and the surface environment.

Our study fully considers the complex correlation between the road network structure and the surface environment, rationally organizing multisource geographic data using a dual-layer complex network model. This approach provides an innovative perspective for assessing urban flood vulnerability. After the successful proposal of the road network flood vulnerability assessment system, the city's flood vulnerability can be analyzed based on a small amount of urban elemental data. This reduces the workload involved in flood assessment and prompts the relevant authorities to accurately and rationally plan and protect high-flood-risk roads.

4.3. Measures to Reduce Flood Vulnerability

According to the results, the overall vulnerability to flooding in Shenzhen is under control, but some areas exhibit higher vulnerability levels. Geographically, the northern and western regions of Shenzhen have a greater vulnerability to flooding, as do certain districts in the south. Regarding roads, those in the southwestern part of Shenzhen are at a higher risk of flooding. Roads such as Caitian Road, Shennan Avenue, Hongli Road, and Xinzhou Road, identified as highly vulnerable, require flood prevention measures to mitigate the risk of flooding disasters. Based on the assessment results, the following measures are proposed to reduce the vulnerability of Shenzhen's transportation system and spatial areas to flooding.

To enhance flood resilience in Shenzhen, strategically placed reservoirs in the northern, western, and southern regions, identified as high-risk areas, can mitigate storm-water

impacts [93]. Coupling this with increased urban greenery could significantly enhance the city's hydrological functionality, promoting sustainable urban drainage and reducing surface runoff.

Critical infrastructure, particularly roads like Caitian Road, Shennan Avenue, Hongli Road, and Xinzhou Road, which are situated in central Shenzhen and are highly vulnerable to flooding, necessitates targeted enhancements. Expanding road widths, integrating permeable materials into pavement designs for better water permeation and storage, and adopting elevated road systems ensure maintenance of essential connectivity during floods, safeguarding key economic zones [94].

Advanced engineering solutions are also vital. Implementing smart drainage systems equipped with real-time monitoring can dynamically manage water flow and storage, optimizing the city's response to flood risks. This adaptation is essential for handling the variable rain intensities associated with climate change [95].

Urban planning should integrate rigorous flood risk assessments in all new developments. These evaluations could inform the development and retrofitting of urban areas to enhance flood resilience, ensuring that infrastructure investments explicitly consider potential flood impacts [96].

Community engagement is crucial for effective flood risk management. Educational programs and participatory planning processes can empower residents, enhancing their capacity to respond to and recover from flood incidents [97].

In summary, the results of this study offer actionable recommendations for urban policymakers on a granular scale. For Shenzhen, the city can reduce its vulnerability and enhance the resilience of its transportation system to flooding by implementing the aforementioned strategies or by taking additional measures.

5. Conclusions

Assessing urban flood disaster vulnerability provides scientific support for disaster prevention and mitigation strategies in cities. Given the significant impact of flooding in Shenzhen, evaluating its flood vulnerability is crucial. To this end, a dual-layer network model for assessing flood vulnerability has been developed and applied to Shenzhen. Based on the model, the spatial and road flood vulnerability of Shenzhen City has been studied as a study area. The main contributions of this study are summarized below:

(1) This study proposes a dual-layer complex network model for evaluating the flood vulnerability of urban transportation systems, and it examines the spatial distribution of flood vulnerability within cities. The model incorporates the complex interplay between road network structures and the ground surface, offering an analysis of road flood disaster vulnerability from the perspective of a multi-layer complex network. Using this model, the study quantitatively assessed and analyzed the flood vulnerability of Shenzhen's road networks and spatial flood vulnerability.

(2) According to the results, the overall vulnerability to flooding in Shenzhen is under control, but some areas exhibit higher vulnerability levels. The spatial distribution of flood vulnerability in Shenzhen City is pronounced, primarily concentrated in the northern and western regions, forming a vulnerability gradient that weakens progressively from west to east. The Nanshan, Futian, and Luohu districts of Shenzhen City are identified as having higher flood vulnerability and are situated in economically developed areas. The roads in Shenzhen with high flood vulnerability are primarily located in the central urban area of the southwest, with ten road sections including the Caitian Road North Section identified as highly vulnerable to flooding, requiring reasonable protection strategies.

(3) The study conducted validation of the model assessment results through waterlogging point verification and proposed recommended preventative measures based on the assessment outcomes. The quantitative results of the model are consistent with the recorded distribution trend in inundation points, indicating that the model outcomes are authentic and reliable.

However, this study is not without its limitations. The model faces challenges in conducting real-time assessments in dynamically changing road network environments. The dynamic construction of roads often affects the results of the network structure and zonal vulnerability analysis. In the future, real-time geographic information can be combined with a dual-layer network model to establish a dynamic dual-layer evaluation network that responds to urban flood vulnerability indicator values in real time.

Author Contributions: Conceptualization: J.D. and Y.W.; data curation: J.D. and Y.W.; formal analysis: J.D. and Y.W.; methodology: J.D.; writing original draft: J.D. and C.L.; and writing review and editing: J.D. and Y.W. All authors have read and agreed to the published version of the manuscript.

Funding: This research was funded by the Fundamental Research Funds for Central Universities, China University of Geosciences (Wuhan), grant number 162301237014.

Data Availability Statement: The partial data for this article are available at the following URLs: https://www.gscloud.cn (accessed on 11 March 2023), http://data.cma.cn/ (accessed on 18 February 2023), https://www.ncei.noaa.gov/ (accessed on 21 July 2023), https://www.worldpop.org/ (accessed on 21 July 2023), and https://www.openstreetmap.org/ (accessed on 6 July 2023). Because of privacy restrictions, additional data are available upon request from the corresponding author.

Conflicts of Interest: The authors declare no conflicts of interest.

References

1. Jha, A.K.; Bloch, R.; Lamond, J. *Cities and Flooding: A Guide to Integrated Urban Flood Risk Management for the 21st Century*; World Bank: Washington, DC, USA, 2012; pp. 46–49. [Google Scholar]
2. Kundzewicz, Z.W.; Kanae, S.; Seneviratne, S.I.; Handmer, J.; Nicholls, N.; Peduzzi, P.; Mechler, R.; Bouwer, L.M.; Arnell, N.; Mach, K. Flood risk and climate change: Global and regional perspectives. *Hydrol. Sci. J.* **2014**, *59*, 1–28. [CrossRef]
3. Zheng, Z.; Qi, S.; Xu, Y. Questionable frequent occurrence of urban flood hazards in modern cities of China. *Nat. Hazards* **2013**, *65*, 1009–1010. [Google Scholar] [CrossRef]
4. Yan, D.; Liu, J.; Shao, W.; Mei, C. Evolution of urban flooding in China. *Proc. Int. Assoc. Hydrol. Sci.* **2020**, *383*, 193–199. [Google Scholar] [CrossRef]
5. Chen, N.; Yao, S.; Wang, C.; Du, W. A method for urban flood risk assessment and zoning considering road environments and terrain. *Sustainability* **2019**, *11*, 2734. [Google Scholar] [CrossRef]
6. Santos, L.B.; Jorge, A.A.; Londe, L.R.; Reani, R.T.; Bacelar, R.B.; Sokolov, I.M. Vulnerability analysis in complex networks under a flood risk reduction point of view. *Front. Phys.* **2023**, *11*, 1064122. [CrossRef]
7. Li, C.; Sun, N.; Lu, Y.; Guo, B.; Wang, Y.; Sun, X.; Yao, Y. Review on Urban Flood Risk Assessment. *Sustainability* **2023**, *15*, 765. [Google Scholar] [CrossRef]
8. Lyu, H.M.; Sun, W.J.; Shen, S.L.; Arulrajah, A. Flood risk assessment in metro systems of mega-cities using a GIS-based modeling approach. *Sci. Total Environ.* **2018**, *626*, 1012–1025. [Google Scholar] [CrossRef] [PubMed]
9. Burton, I.; Kates, R.W.; White, G.F. *The Environment as Hazard*, 2nd ed.; Guilford: New York, NY, USA, 1993. [Google Scholar]
10. Chubey, M.S.; Hathout, S. Integration of RADARSAT and GIS modelling for estimating future Red River flood risk. *GeoJournal* **2004**, *59*, 237–246. [Google Scholar] [CrossRef]
11. Xia, J.; Dong, B.; Li, Q.; Liu, L.; Zhou, M.; Wang, X. Hydrodynamic mechanism analysis and disaster reduction countermeasures of urban flood disaster in recent years. *China Flood Drought Manag.* **2022**, *32*, 66–71. [Google Scholar]
12. Tong, J.; Zhang, H.; Liu, H.; Huang, J.; Hao, Y. XGBoost-based waterlogging risk assessment and influencing factors analysis of core cities in Yangtze River Delta. *Water Resour. Hydropower Eng.* **2021**, *52*, 1–11. [Google Scholar]
13. Kron, W. Flood risk = hazard • values • vulnerability. *Water Int.* **2005**, *30*, 58–68. [Google Scholar] [CrossRef]
14. Field, C.B.; Barros, V.; Stocker, T.F.; Dahe, Q. *Managing the Risks of Extreme Events and Disasters to Advance Climate Change Adaptation: Special Report of the Intergovernmental Panel on Climate Change;* Cambridge University Press: Cambridge, UK, 2012; ISBN 1-107-02506-0. [Google Scholar]
15. Yin, J.; Ye, M.; Yin, Z.; Xu, S. A review of advances in urban flood risk analysis over China. *Stoch. Environ. Res. Risk Assess.* **2014**, *29*, 1063–1070. [Google Scholar] [CrossRef]
16. Mechler, R.; Bouwer, L.M.; Linnerooth-Bayer, J.; Hochrainer-Stigler, S.; Aerts, J.C.J.H.; Surminski, S.; Williges, K. Managing unnatural disaster risk from climate extremes. *Nat. Clim. Chang.* **2014**, *4*, 235–237. [Google Scholar] [CrossRef]
17. Wang, Y.; Chen, X.; Wang, L. Differential Semi-Quantitative Urban Risk Assessment of Storm Surge Inundation. *ISPRS Ann. Photogramm. Remote Sens. Spat. Inf. Sci.* **2022**, *X-3/W1-2022*, 177–185. [Google Scholar] [CrossRef]
18. Salman, A.M.; Li, Y. Flood risk assessment, future trend modeling, and risk communication: A review of ongoing research. *Nat. Hazards Rev* **2018**, *19*, 04018011. [Google Scholar] [CrossRef]
19. Wang, X.; Zhang, Z.; Hu, W.; Zhao, X.; Qi, X.; Cai, R. Vulnerability Assessment and Future Prediction of Urban Waterlogging—A Case Study of Fuzhou. *Water* **2023**, *15*, 4025. [Google Scholar] [CrossRef]

20. Birkmann, J.; Cardona, O.D.; Carreño, M.L.; Barbat, A.H.; Pelling, M.; Schneiderbauer, S.; Kienberger, S.; Keiler, M.; Alexander, D.; Zeil, P.; et al. Framing vulnerability, risk and societal responses: The MOVE framework. *Nat. Hazards* **2013**, *67*, 193–211. [Google Scholar] [CrossRef]
21. Chen, W.; Li, X.; Wang, L. Multimodal Remote sensing science and technology. In *Remote Sensing Intelligent Interpretation for Mine Geological Environment: From Land Use and Land Cover Perspective*; Springer: Singapore, 2022; pp. 7–32.
22. Moreira, L.L.; De Brito, M.M.; Kobiyama, M. Review article: A systematic review and future prospects of flood vulnerability indices. *Nat. Hazards Earth Syst. Sci. Discuss.* **2021**, *21*, 1513–1530. [Google Scholar] [CrossRef]
23. Nasiri, H.; Mohd Yusof, M.J.; Mohammad Ali, T.A. An overview to flood vulnerability assessment methods. *Sustain. Water Resour. Manag.* **2016**, *2*, 331–336. [Google Scholar] [CrossRef]
24. Brouwer, R.; Akter, S.; Brander, L.; Haque, E. Socioeconomic vulnerability and adaptation to environmental risk: A case study of climate change and flooding in Bangladesh. *Risk Anal.* **2007**, *27*, 313–326. [Google Scholar] [CrossRef]
25. Suarez, P.; Anderson, W.; Mahal, V.; Lakshmanan, T.R. Impacts of flooding and climate change on urban transportation: A system wide performance assessment of the Boston Metro Area. *Transp. Res.* **2005**, *10*, 231–244. [Google Scholar] [CrossRef]
26. Li, J.; Gao, J.; Li, N.; Yao, Y.; Jiang, Y. Risk Assessment and Management Method of Urban Flood Disaster. *Water Resour. Manag.* **2023**, *37*, 2001–2018. [CrossRef] [CrossRef]
27. Mattsson, L.G.; Jenelius, E. Vulnerability and resilience of transport systems—A discussion of recent research. *Transp. Res. Part A Policy Pract.* **2015**, *81*, 16–34. [Google Scholar] [CrossRef]
28. Yerra, B.M.; Levinson, D.M. The emergence of hierarchy in transportation networks. *Ann. Reg. Sci.* **2005**, *39*, 541–553. [Google Scholar] [CrossRef]
29. Lin, J.; Lin, W. Transportation System Vulnerability Assessment Considering Environmental Impact. *J. Adv. Transp.* **2022**, *2022*, 8711894. [Google Scholar] [CrossRef]
30. Balijepalli, C.; Oppong, O. Measuring vulnerability of road network considering the extent of serviceability of critical road links in urban areas. *J. Transp. Geogr.* **2014** , *39*, 145–155. [Google Scholar] [CrossRef]
31. Santos, L.B.; Jorge, A.A.; Londe, L.R.; Reani, R.T.; Bacelar, R.B.; Sokolov, I.M. Vulnerability analysis in Complex Networks under a Flood Risk Reduction point of view. *Nat. Hazards Earth Syst. Sci. Discuss.* **2019**, 2019, 1–8. [Google Scholar] [CrossRef]
32. Abdulla, B.; Mostafavi, A.; Birgisson, B. Characterization of the vulnerability of road networks to fluvial flooding using network percolation approach. In *Computing in Civil Engineering 2019: Smart Cities, Sustainability, and Resilience*; American Society of Civil Engineers: Reston, VA, USA, 2019; pp. 428–435. [Google Scholar]
33. Singh, P.; Sinha, V.S.P.; Vijhani, A.; Pahuja, N. Vulnerability assessment of urban road network from urban flood. *Int. J. Disaster Risk Reduct.* **2018**, *28*, 237–250. [Google Scholar] [CrossRef]
34. Rong, Y.; Zhang, T.; Zheng, Y.; Hu, C.; Peng, L.; Feng, P. Three-dimensional urban flood inundation simulation based on digital aerial photogrammetry. *J. Hydrol.* **2020**, *584*, 124308. [Google Scholar] [CrossRef]
35. Marulanda, M.; De la Llera, J.; Cardona, O.D. A macroeconomic disaster risk analysis: The case study of Chile. *Int. J. Disaster Risk Reduct.* **2022**, *74*, 102875. [Google Scholar] [CrossRef]
36. Koks, E.E.; Rozenberg, J.; Zorn, C.; Tariverdi, M.; Vousdoukas, M.; Fraser, S.A.; Hall, J.; Hallegatte, S. A global multi-hazard risk analysis of road and railway infrastructure assets. *Nat. Commun.* **2019**, *10*, 2677. [Google Scholar] [CrossRef]
37. Ma, Y.; Wu, H.; Wang, L.; Huang, B.; Ranjan, R.; Zomaya, A.; Jie, W. Remote sensing big data computing: Challenges and opportunities. *Future Gener. Comput. Syst.* **2015**, *51*, 47–60. [Google Scholar] [CrossRef]
38. Pricope, N.G.; Halls, J.N.; Rosul, L.M.; Hidalgo, C. Residential Flood Vulnerability Along the Developed North Carolina, USA Coast: High Resolution Social and Physical Data for Decision Support. *Data Brief* **2019**, *24*, 103975. [Google Scholar] [CrossRef] [PubMed]
39. Jia, H.C.; Chen, F.; Zhang, J.; Du, E.Y. Vulnerability analysis to drought based on remote sensing indexes. *Int. J. Environ. Res. Public Health.* **2020**, *17*, 7660. [Google Scholar] [CrossRef] [PubMed]
40. Luenam, A.; Puttanapong, N. Modelling and Analyzing Spatial Clusters of Leptospirosis Based on Satellite-Generated Measurements of Environmental Factors in Thailand During 2013–2015. *Geospat. Health* **2020**, *15*, 2. [Google Scholar] [CrossRef]
41. Cohen, J.M.; Ernst, K.C.; Lindblade, K.A.; Vulule, J.M.; John, C.C.; Wilson, M.L. Topography-derived wetness indices are associated with household-level malaria risk in two communities in the western Kenyan highlands. *Malar. J.* **2008**, *7*, 40. [Google Scholar] [CrossRef]
42. Reid, C.E.; O'Neill, M.S.; Gronlund, C.J.; Brines, S.J.; Brown, D.G.; Diez-Roux, A.V.; Schwartz, J. Mapping community determinants of heat vulnerability. *Environ. Health Perspect.* **2009**, *117*, 1730–1736. [Google Scholar] [CrossRef]
43. Liu, H.; Behr, J.G.; Diaz, R. Population vulnerability to storm surge flooding in coastal Virginia, USA. *Integr. Environ. Assess. Manag.* **2016**, *12*, 500–509. [Google Scholar] [CrossRef] [PubMed]
44. Keay, K.; Simmonds, I. The association of rainfall and other weather variables with road traffic volume in Melnnourne, Australia. *Accid. Anal. Prev.* **2005**, *37*, 109–124. [Google Scholar] [CrossRef]
45. Wu, W.-B.; Ma, J.; Banzhaf, E.; Meadows, M.E.; Yu, Z.-W.; Guo, F.-X.; Sengupta, D.; Cai, X.-X.; Zhao, B. A first Chinese building height estimate at 10 m resolution (CNBH-10 m) using multi-source earth observations and machine learning. *Remote Sens. Environment.* **2023**, *291*, 113578. [Google Scholar] [CrossRef]
46. Yang, J.; Huang, X. The 30 m Annual Land Cover Dataset and Its Dynamics in China from 1990 to 2019. *Earth Syst. Sci. Data* **2021**, *13*, 3907–3925. [Google Scholar] CrossRef] [CrossRef]

47. Chen, H.; Shi, H.-L. The impact of network topological structures on systematic technology adoption and carbon emission reduction. *Sci. Rep.* **2021**, *11*, 20380. [CrossRef]
48. Huang, X.; Li, H.; Zhang, Y.; Yang, X.; Chen, S. Construction of urban waterlogging vulnerability assessment system and vulnerability assessment based on PSR & AHP method in Xi'an city. *J. Nat. Disasters* **2019**, *28*, 167–175. [Google Scholar]
49. Bertilsson, L.; Wiklund, K.; de Moura Tebaldi, I.; Rezende, O.M.; Veról, A.P.; Miguez, M.G. Urban flood resilience–A multi-criteria index to integrate flood resilience into urban planning. *J. Hydrol.* **2019**, *573*, 970–982. [CrossRef]
50. Li, M.; Sun, H.; Singh, V.P.; Zhou, Y.; Ma, M. Agricultural water resources management using maximum entropy and entropy-weight-based TOPSIS methods. *Entropy*. **2019**, *21*, 364. [CrossRef]
51. Chen, P. Effects of Normalization on the Entropy-Based TOPSIS Method. *Expert Syst. Appl.* **2019**, *136*, 33–41. [Google Scholar] [CrossRef]
52. Al-Aomar, R. A Combined AHP-Entropy Method for Deriving Subjective and Objective Criteria Weights. *Int. J. Ind. Eng. Theory Appl. Pract*. **2010**, *17*, 12–24. [Google Scholar]
53. Beiler, M.R.O.; Treat, C. Integrating GIS and AHP to Prioritize Transportation Infrastructure Using Sustainability Metrics. *J. Infrastruct. Syst.* **2015**, *21*, 04014053. [Google Scholar] [CrossRef]
54. Behzadian, M.; Otaghsara, S.K.; Yazdani, M.; Ignatius, J. A state-of the-art survey of TOPSIS applications. *Expert Syst. Appl.* **2012**, *39*, 13051–13069. [Google Scholar] [CrossRef]
55. Salih, M.; Zaidan, B.; Zaidan, A.; Ahmed, M. Survey on fuzzy TOPSIS state-of-the-art between 2007 and 2017. *Comput. Oper. Res.* **2019**, *104*, 207–227. [Google Scholar] [CrossRef]
56. Saroj, K. Review: Study on simple k mean and modified K mean clustering technique. *Int. J. Comput. Sci. Eng. Technol*. **2016**, *6*, 279–281. [Google Scholar]
57. Na, S.; Xumin, L.; Yong, G. Research on k-means clustering algorithm: An improved k-means clustering algorithm. In Proceedings of the 2010 Third International Symposium on Intelligent Information Technology and Security Informatics, Jian, China, 2–4 April 2010; pp. 63-67. [Google Scholar]
58. Farahmand, H.; Xu, Y.; Mostafavi, A. A spatial–temporal graph deep learning model for urban flood nowcasting leveraging heterogeneous community features. *Sci. Rep.* **2023**, *13*, 6768. [CrossRef] [PubMed]
59. Shughrue, C.; Seto, K.C. Systemic vulnerabilities of the global urban-industrial network to hazards. *Clim. Chang.* **2018**, *151*, 173–187. [Google Scholar] [CrossRef]
60. Ukkusuri, S.V.; Yushimito, W.F. A methodology to assess the criticality of highway transportation networks. *J. Transp. Secur.* **2009**, *2*, 29–46. [Google Scholar] [CrossRef]
61. Reggiani, A.; Nijkamp, P.; Lanzi, D. Transport resilience and vulnerability: The role of connectivity. *Transp. Res. Part A Policy Pract.* **2015**, *81*, 4–15. [Google Scholar] [CrossRef]
62. Pregnolato, M.; Ford, A.; Wilkinson, S.M.; Dawson, R.J. The impact of flooding on road transport: A depth-disruption function. *Transp. Res. Part D Transp. Environ.* **2017**, *55*, 67–81. [Google Scholar] [CrossRef]
63. Zhou, R.; Zheng, H.; Liu, Y.; Xie, G.; Wan, W. Flood impacts on urban road connectivity in southern China. *Sci. Rep.* **2022**, *12*, 16866. [CrossRef] [PubMed]
64. Sharma, S.; Ram, S. Investigation of Road Network Connectivity and Accessibility in Less Accessible Airport Regions: The Case of India. *Sustainability* **2023**, *15*, 5747. [Google Scholar] CrossRef] [CrossRef]
65. Bell, M.G.H. A game theory approach to measuring the performance reliability of transport networks. *Transp. Res. Part B Methodol.* **2000**, *34*, 533–545. [Google Scholar] [CrossRef]
66. Berche, B.; Von Ferber, C.; Holovatch, T.; Holovatch, Y. Resilience of public transport networks against attacks. *Eur. Phys. J. B* **2009**, *71*, 125–137. [Google Scholar] [CrossRef]
67. Taylor, M.A.P.; D'Este, G.M. Transport Network Vulnerability: A Method for Diagnosis of Critical Locations in Transport Infrastructure Systems. *Adv. Spat. Sci.* **2007**, *2*, 9–30. [Google Scholar] [CrossRef]
68. Yen, J.Y. An algorithm for finding shortest routes from all source nodes to a given destination in general networks. *Q. Appl. Math.* **1970**, *27*, 526–530. [Google Scholar] [CrossRef]
69. Strasser, B.; Wagner, D.; Zeitz, T. Space-Efficient, Fast and Exact Routing in Time-Dependent Road Networks. *Alorithms* **2021**, *14*, 90. [Google Scholar] [CrossRef]
70. Shi, C.Y.; Chen, B.Y.; Lam, W.H.K.; Li, Q.Q. Heterogeneous data fusion method to estimate travel time distributions in congested road networks. *Transp. Res. B Methodol*. **2017**, *17*, 2822. [Google Scholar] [CrossRef] [PubMed]
71. Zhang, X.; Miller-Hooks, E.; Denny, K. Assessing the Role of Network Topology in Transportation Network Resilience. *J. Transp. Geogr.* **2015**, *46*, 35–45. [Google Scholar] [CrossRef]
72. Latora, V.; Marchiori, M. Efficient behavior of small-world networks. *Phys. Rev. Lett.* **2001**, *87*, 198701. [Google Scholar] [CrossRef] [PubMed]
73. Kalinic, M.; Krisp, J.M. Fuzzy inference approach in traffic congestion detection. *Ann. GIS* **2019**, *25*, 329–336. [Google Scholar] [CrossRef]
74. Mitsakis, E.; Salanova Grau, J.M.; Chrysohoou, E.; Stamos, I.; Aifandopoulou, G. Multi-criteria route choice in road networks. *Int. J. Inf. Decis. Sci.* **2015**, *7*, 3–17. [Google Scholar] [CrossRef]
75. Zhou, Y.; Sheu, J.B.; Wang, J. Robustness assessment of urban road network with consideration of multiple hazard events. *Risk Anal.* **2017**, *37*, 1477–1494. [Google Scholar] [CrossRef] [PubMed]

76. Cao, W.; Yang, Y.; Huang, J.; Sun, D.; Liu, G. Influential Factors Affecting Protective Coping Behaviors of Flood Disaster: A Case Study in Shenzhen, China. *Int. J. Environ. Res. Public Health* **2020**, *17*, 5945. [Google Scholar] [CrossRef] [PubMed]
77. Cheng, L.; Wang, L.; Feng, R. Fractal Characteristics and Evolution of Urban Land-Use: A Case Study in the Shenzhen City (1988–2015). In Proceedings of the IGARSS 2020–2020 IEEE International Geoscience and Remote Sensing Symposium, Waikoloa, HI, USA, 26 September–2 October 2020; pp. 4275–4278. [Google Scholar] [CrossRef]
78. Wang, Y.; Chen, X.; Wang, L. Deep Reinforcement Learning-Based Rescue Resource Distribution Scheduling of Storm Surge Inundation Emergency Logistics. *IEEE Trans. Ind. Inform.* **2023**, *19*, 10004–10013. [Google Scholar] [CrossRef]
79. Zhou, L.; Wu, X.; Ji, Z.; Gao, G. Characteristic analysis of rainstorm-induced catastrophe and the countermeasures of flood hazard mitigation about Shenzhen city. *Geomat. Nat. Hazards Risk* **2017**, *8*, 1886–1897. [CrossRef]
80. Zacharias, J.; Tang, Y. Restructuring and repositioning Shenzhen, China's new mega city. *Prog. Plan.* **2010**, *73*, 209–249. [CrossRef]
81. Chen, P.; Zhang, J.; Zhang, L.; Sun, Y. Evaluation of resident evacuations in urban rainstorm waterlogging disasters based on scenario simulation: Daoli district (Harbin, China) as an example. *Int. J. Environ. Res. Public Health.* **2014**, *11*, 9964–9980. [CrossRef] [PubMed]
82. Hoque, M.A.; Tasfia, S.; Ahmed, N.; Pradhan, B. Assessing spatial flood vulnerability at Kalapara Upazila in Bangladesh using an analytic hierarchy process. *Sensors*. **2019**, *19*, 1302. [CrossRef] [PubMed]
83. Tayyab, M.; Zhang, J.; Hussain, M.; Ullah, S.; Liu, X.; Khan, S.N.; Baig, M.A.; Hassan, W.; Al-Shaibah, B. Gis–based urban flood resilience assessment using urban flood resilience model: A case study of peshawar city, khyber pakhtunkhwa, pakistan. *Remote Sens*. **2021**, *13*, 1864. [CrossRef]
84. Saroj, N.; Chatterjee, S.; Das Adhikari, M. Integrated remote sensing and GIS based spatial modelling through analytical hierarchy process (AHP) for water logging hazard, vulnerability and risk assessment in Keleghai river basin, India. *Model. Earth Syst. Environ*. **2015**, *1*, 31. [CrossRef]
85. Ghosh, T.; Powell, R.L.; Elvidge, C.D.; Baugh, K.E.; Sutton, P.C.; Anderson, S. Shedding Light on the Global Distribution of Economic Activity. *Open Geogr. J.* **2010**, *3*, 147–160. [CrossRef]
86. Chen, J.L.; Chen, W.J.; Huang, G.R. Urban Waterlogging Risk Assessment Based on Scenario Simulation and Multi-source Data. *Water Resour. Power*. **2021**, *39*, 55–59. [Google Scholar]
87. Jenelius, E. Network structure and travel patterns: Explaining the geographical disparities of road network vulnerability. *J. Transp. Geogr.* **2009**, *17*, 234–244. [CrossRef]
88. Herman, R.; Ardekani, S. Characterizing traffic conditions in urban areas. *Transp. Sci.* **1984**, *18*, 101–140. [CrossRef]
89. Wang, S.; Han, W.; Huang, X.; Zhang, X.; Wang, L.; Li, J. Trustworthy remote sensing interpretation: Concepts, technologies, and applications. *ISPRS J. Photogramm. Remote Sens.* **2024**, *209*, 150–172. [Google Scholar] [CrossRef]
90. Wang, L.; Zuo, B.; Le, Y.; Chen, Y.; Li, J. Penetrating remote sensing: Next-generation remote sensing for transparent earth. *Innovation* **2023**, *4*, 100519. [Google Scholar] [CrossRef]
91. MS, M.; Katpatal, Y.B.; Londhe, D.S. Measurement of city road network resilience in hazardous flood events. *Int. J. Disaster Resil. Built Environ.* **2024**, *15*, 274–288. [Google Scholar] [CrossRef]
92. Drejza, S.; Bernatchez, P.; Marie, G.; Friesinger, S. Quantifying road vulnerability to coastal hazards: Development of a synthetic index. *Ocean. Coast. Manag.* **2019**, *181*, 104894. [Google Scholar] [CrossRef]
93. Tingsanchali, T. Urban flood disaster management. *Procedia Eng*. **2012**, *32*, 25–37. [Google Scholar] [CrossRef]
94. Yereseme, A.K.; Surendra, H.J.; Kuntoji, G. Sustainable integrated urban flood management strategies for planning of smart cities: A review. *Sustain. Water Resour. Manag*. **2022**, *8*, 85. [Google Scholar] [CrossRef]
95. Willems, P.; Arnbjerg-Nielsen, K.; Olsson, J.; Nguyen, V.T.V. Climate change impact assessment on urban rainfall extremes and urban drainage: Methods and shortcomings. *Atmos. Res.* **2012**, *103*, 106–118. [Google Scholar] [CrossRef]
96. Gersonius, B.; Ashley, R.; Pathirana, A.; Zevenbergen, C. Climate Change Uncertainty: Building Flexibility into Water and Flood Risk Infrastructure. *Clim. Chang*. **2013**, *116*, 411–423. [Google Scholar] [CrossRef]
97. Alfieri, L.; Burek, P.; Feyen, L.; Forzieri, G. Global warming increases the frequency of river floods in Europe. *Hydrol. Earth Syst. Sci*. **2015**, *19*, 2247–2260. [Google Scholar] [CrossRef]

Disclaimer/Publisher's Note: The statements, opinions and data contained in all publications are solely those of the individual author(s) and contributor(s) and not of MDPI and/or the editor(s). MDPI and/or the editor(s) disclaim responsibility for any injury to people or property resulting from any ideas, methods, instructions or products referred to in the content.